

ClipRover: Zero-shot Vision-Language Exploration and Target Discovery by Mobile Robots

Yuxuan Zhang¹, Adnan Abdullah², Sanjeev J. Koppal^{*3}, and Md Jahidul Islam^{*4}

*Equal Contribution ^{†‡}

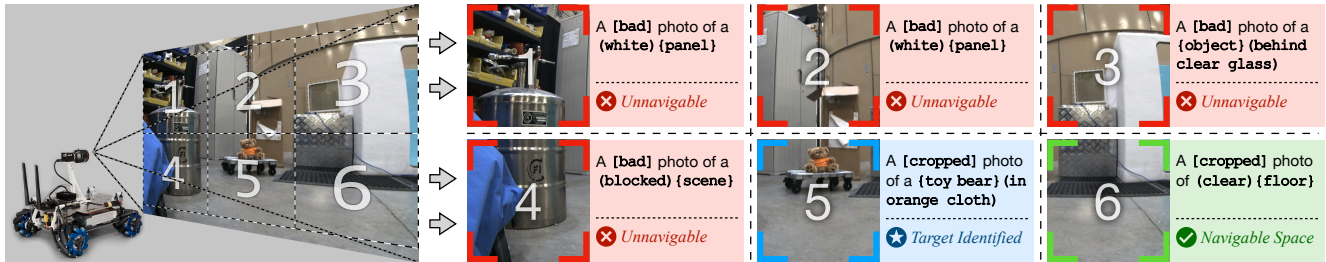


Figure 1. Illustration of an ongoing exploration and target discovery task by the proposed ClipRover system. **Left:** A synthesized image representing the robot’s onboard camera; the cone illustrates its field-of-view, divided into six numbered tiles for detailed analysis. **Right:** The vision-language perception of each tile is processed by a novel correlation middleware; The motion mixer engine is currently in ‘target lock’ mode, prioritizing the target (a teddy bear) in tile-5 over other navigable regions (e.g., tile-6) due to the higher precedence assigned to the target. Full demo is available at the project page: <https://robopi.ece.ufl.edu/cliprover.html>.

Abstract

Vision-language navigation (VLN) has emerged as a promising paradigm, enabling mobile robots to perform zero-shot inference and execute tasks without specific pre-programming. However, current systems often separate map exploration and path planning, with exploration relying on inefficient algorithms due to limited (partially observed) environmental information. In this paper, we present a novel navigation pipeline named “ClipRover” for simultaneous exploration and target discovery in unknown environments, leveraging the capabilities of a vision-language model named CLIP. Our approach requires only monocular vision and operates without any prior map or knowledge about the target. For comprehensive evaluations, we design the functional prototype of a UGV (unmanned ground vehicle) system named “Rover Master”, a customized platform for general-purpose VLN tasks. We integrate and deploy the ClipRover pipeline on Rover Master to evaluate its throughput, obstacle avoidance capability, and trajectory performance across various real-world scenarios. Experimental results demonstrate that ClipRover consistently outperforms traditional map traversal algorithms and achieves performance comparable to

path-planning methods that depend on prior map and target knowledge. Notably, ClipRover offers real-time active navigation without requiring pre-captured candidate images or pre-built node graphs, addressing key limitations of existing VLN pipelines.

Keywords. Vision-Language Navigation; Zero-Shot Visual Servoing; Path Planning; GPS-denied Navigation.

1. Introduction

Autonomous exploration and target discovery is a fundamental problem in robotics, with applications ranging from search-and-rescue to environmental monitoring and surface mapping [43, 70]. In 2D exploration, notable implementations are seen in household robots, e.g., vacuum cleaning [23, 65] and warehouse robotics [16, 34]. Traditionally, their navigation strategies have relied on various forms of *Bug algorithms* (Bug0, Bug1, Bug2) [45, 47], which are best suited when a robot has *a priori* belief about the environment, and can sense obstacles locally. The principle is to use the *line-of-sight* gradient towards the goal by applying simple obstacle avoidance schemes. Algorithms such as *random walks* or predefined *search patterns* are also utilized to explore an unknown workspace to develop an *occupancy* grid map, on which standard path-planning algorithms [3, 69] can be deployed for mobile robot navigation. Tree search algorithms like Dijkstra and A* [9] have been popular as they are simple and efficient for limited onboard

[†]^{2,4}RoboPI Laboratory, Dept. of ECE, University of Florida (UF)

[†]^{1,3}FOCUS Laboratory, Dept. of ECE, University of Florida (UF)

[†]³Amazon Robotics (Dr. Koppal holds concurrent appointments as an Associate Professor of ECE-UF and an Amazon Scholar at Amazon Robotics. This project is performed at UF, not associated with Amazon.)

resources [73]. For large search spaces, sampling-based methods such as Probabilistic Roadmaps (PRM) [33] and Rapidly-exploring Random Tree (RRT) [39] and RRT* [32] are generally adopted for source-to-target path planning in real-time.

In existing unmanned ground vehicle (UGV) systems, mapping and target discovery are typically conducted as separate processes, relying on different sensors. For instance, a 2D LiDAR is commonly used for obstacle avoidance and mapping [57, 66], while a separate camera is used for scene classification and target detection [35]. In a more complicated 3D environment such as an underwater cave exploration, the robot may need to use a combination of sensors such as sonar, LiDAR, and cameras to navigate and explore the environment by generating a semantic representation of the surroundings [1, 59]. However, an initial map traversal is not feasible in partially observable and dynamic environments, requiring frequent correction or re-initialization [7, 24].

More advanced UGV systems address this by using *on-line* path planning algorithms [53, 54] with dynamic obstacles and partially observable state space. The major challenge here is to adapt the path when new obstacles intersect the trajectory and/or dynamic changes occur in the environment [13]. To this end, visually-guided robots use the semantic understanding and spatio-temporal modeling of dynamic objects in the scene [26, 50]. For visual semantic navigation, the path planner becomes an intermediate representation of a *task planner* [60] for application-specific higher-level tasks such as inspection [72] search-and-rescue [71], exploration [41], *etc.* In recent years, more *interactive* task planners are designed with vision-language navigation (VLN) models [17, 25] to enable human-like understanding of the robot’s tasks from natural language and visual (semantic) cues. These are particularly useful for human-in-the-loop systems [28], *e.g.*, robots operating in warehouses, healthcare, and social settings. VLNs enable robots to interpret the *context* of the tasks from language description and map the corresponding visual *cues* to make context-aware navigation decisions. However, integrating vision-language models (VLMs) into the early stages of map exploration – remains unexplored. We hypothesize that this integration can enable robots to leverage high-level zero-shot visual information for **simultaneous exploration and target discovery** without a prior map.

This paper presents **ClipRover**, a novel framework that utilizes the spatial context awareness capabilities of general-purpose VLMs [10] to guide robotic exploration and target discovery in unknown environments. The framework adopts a modular architecture organized into three key stages: *perception*, *correlation*, and *decision*. This modular design enables the decomposition of complex system-level challenges into smaller, manageable sub-problems, al-

lowing for iterative improvements to each stage. Furthermore, the framework features a highly configurable correlation middleware, offering flexibility to adapt to various tasks and environmental conditions without any prior map or knowledge about the target.

To validate the proposed framework in real-world environments, we develop a UGV platform that meets the computational demands of VLMs while offering superior maneuverability and mechanical stability during the task. We deployed the CLIP model [27, 58] in our proposed architecture and performed extensive tests in a real-world environment. Overall, we make the following contributions to this paper:

1. **Science:** We propose a novel navigation pipeline named ClipRover for simultaneous exploration and target discovery by UGVs in unknown environments. It harnesses the power of VLMs into a modular architecture, consisting of a vision-encoder as *frontend*, language correlation databases as *middlewares*, and a decision-maker as the *backend*.
2. **System:** We design a novel UGV platform to support the maneuverability and computational demands of VLM-based navigation systems like ClipRover. It is designed to be powerful and configurable for general-purpose robotics research; it will be open-sourced for academic use.
3. **Integration:** We develop a fully functional system integrating the proposed navigation pipeline with the UGV platform. It is then optimized for real-time performance through comprehensive benchmarks. We present the key challenges and practicalities involved in deploying such systems in real-world application scenarios.

We conducted extensive experiments to evaluate the proposed system against both map-traversal and path-finding algorithms. A performance comparison based on efficiency and success rates is shown in Fig. 2, identifying four equipotential lines: EP0-EP3. In our evaluation, we observe that algorithms that use a similar amount of information tend to reside on the same EP. A higher equipotential line represents more information (*e.g.*, prior map of the environment, target location, additional sensors) available to the algorithm. With zero prior information of the environment (EP0), ClipRover offers performance margins comparable and often better than Bug2 (EP2-EP3). Note that Bug2 needs prior information on the target position and a precise localization to keep track of its *m-line*. Overall, ClipRover delivers **33% more efficient** source-to-target paths compared to Bug2 and achieves a **10% higher success** than the Bug1 algorithm. Importantly, none of the evaluated planner and traversal methods have a semantic understanding of the scene, limiting their ability to adapt to dynamic environments.

With vision-language integration, SOTA systems such

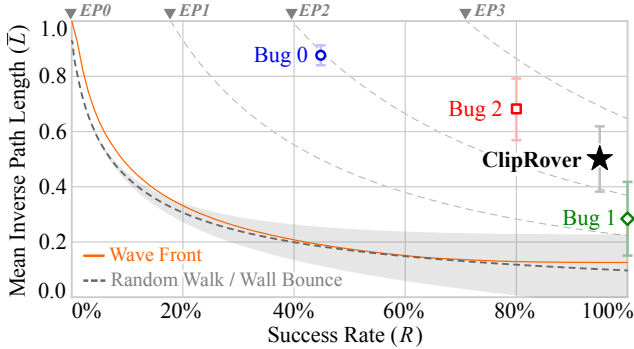


Figure 2. Performance of **ClipRover** compared to map-traversal (e.g., wavefront, random walk, wall bounce) [56] and path-finding (Bug) algorithms [45, 47] for UGV navigation. The equipotential lines labeled as EP^* are defined by Eq. 6.

as Clip-Nav [14], Clip of Wheels [17], and GCN [36] - demonstrate superior navigation performance while providing semantic scene understanding. However, these systems rely on pre-captured images of candidate scenes, target locations, and pre-built knowledge graphs of the navigable space [11]. Additionally, many are tested primarily in simulation or overly simplistic environments. Other contemporary methods, such as SEEK [19], require high-sensing modalities involving multiple cameras, LiDAR, and onboard SLAM pipelines for navigation. ClipRover overcomes these limitations by enabling real-time active navigation using only a monocular camera, without relying on any prior information or pre-built dependencies.

2. Background & Related Work

2.1. Path Planning & Exploration by Mobile Robots

A substantial body of literature has explored various tree search and probabilistic sampling methods for *source-to-goal* path planning and navigation by UGVs and ASVs [42, 61]. Breadth-First Search (BFS) and Depth-First Search (DFS) are generally adopted for *uninformed* search, whereas Dijkstra’s algorithm and A* are widely used for *informed* search [12]. DFS is generally more memory-efficient than BFS and better suited for dynamic obstacles, whereas Dijkstra’s algorithm is ideal when finding the shortest path is essential. Nevertheless, these methods employ exhaustive search, hence can be computationally demanding in complex spaces. The family of A* and D* algorithms [2, 15, 22] improves upon the computational efficiency by incorporating heuristics to reduce unnecessary exploration while guaranteeing the shortest path.

Beyond a discretized grid-like environment, sampling-based algorithms are better suited for continuous high-dimensional spaces [12]. Probabilistic Roadmaps (PRM) [33] and Rapidly-exploring Random Tree (RRT) [39] methods are classical methods that build a

tree of random samples from the configuration space, starting from the initial position and incrementally growing toward the goal [74]. PRM is best for multi-query planning in static environments, whereas RRT is fast and suitable for real-time planning but produces suboptimal paths. While some variants, such as RRT*, are asymptotically optimal, although at a higher computational cost [64].

On the other hand, Bug0 [45] and Bug1 [47] algorithms employ a locally optimal strategy of following the line-of-sight and avoiding obstacles along their boundaries. Bug2 [47] optimizes the path using an imaginary *m-line* (main line) to avoid unnecessary loops. Besides, Alg1 and Alg2 approaches [62] leverage memory of the previous obstacle *hit points* to search for alternative routes, while Dist-Bug [30] makes it memory efficient by retaining the most recent hit points only. M-Bug [54] minimizes the path length by dynamically adjusting the *m-line*. Integration of range sensors further allows the robot to sense nearby obstacles and choose a short-cut while maintaining minimum deviation from *m-line*, as demonstrated in TangentBug [31], WedgeBug [38], and VisBug [46].

In contrast, I-Bug [68] solely relies on signal intensity from the goal to guide navigation. EgressBug [21] offers an escape mechanism, allowing the robot to recover from deadlocks. PointBug [8] introduces the notion of *sudden points*, i.e., turning points on the outer perimeter of obstacles, which is further improved in E-bug methods [52, 53]. More sophisticated algorithms such as APF-Bug [72] assess ground quality to avoid immobilization in complex terrain obstacles and increase the success rate of reaching the goal.

2.2. Zero-shot Learning & Vision-Language Navigation

Zero-shot learning enables autonomous robots to identify unseen objects and make navigation decisions in unfamiliar environments [20]. Researchers use visual features [75], knowledge graphs [55], semantic embeddings [77], and spatial appearance attributes [48] to encode information of object classes into the search space. More recently, text-based descriptions or human instructions are combined with vision to improve servoing, as demonstrated in LM-Nav [63] and InstructNav [44]. Among CLIP [58]-based frameworks, CoW [18] presents a trajectory planning strategy using frontier-based exploration. ClipNav [14] designs a *costmap* to further improve obstacle avoidance during exploration. Other approaches such as ESC [79] and VLMaps [25] use prompts to translate action commands into a sequence of open-vocabulary navigation tasks for planning. Besides, CorNav [40] includes environmental feedback in the zero-shot learning process to dynamically adjust navigation decisions on the fly.

Contemporary works on vision-language navigation (VLN) focus on enabling robots to understand language in-

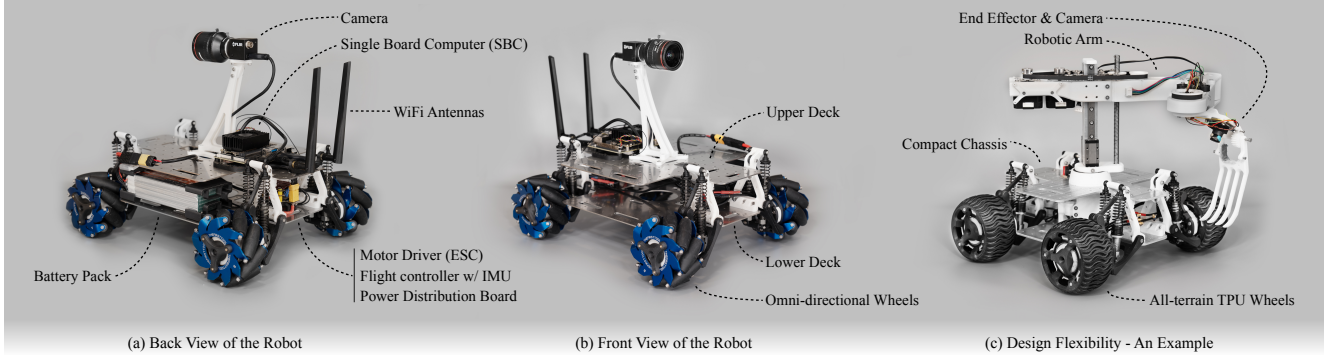


Figure 3. Our *Rover Master* platform designed for ClipRover is shown: **(a)** Back view, showing the single board computer (SBC) and electronics stack including a brushless motor speed controller, a flight controller with IMU, and a power distribution board; **(b)** Front view, showing the camera for zero-shot navigation; **(c)** An alternative design, demonstrating the flexibility of this platform, configured with revised wheels, chassis, and additional manipulators for potential field robotics applications.

structions for interactive task planning. VLN algorithms integrate visual information (*e.g.*, recognizing objects, obstacles) and language instructions to plan a trajectory or action sequence for task execution. This is achieved by first generating semantic tags into the SLAM pipeline [17, 20, 25] to generate a 3D map. Subsequently, the resulting augmented map is used to support online navigation to perform zero-shot semantic tasks [76]. These works primarily focus on adding semantic information to existing mapping and exploration techniques [25, 37], do not participate in the path planning process.

In contrast, *node graph* based VLNs [6, 11, 36] construct a graph of the active map where each node represents a free location and edges stand for directly navigable paths. Dynamic expansion of a node graph is then achieved with the help of precise localization, typically achieved by additional sensors. Experiments show that these algorithms suffer from miscorrelating existing nodes when revisiting an explored area, and also in dynamically changing scenes. To address this, researchers are exploring zero-shot learning aided observation of unknown spaces [76]. Techniques like odometry, stereo depth, and LiDAR sensors are used alongside a pretrained vision-language model to achieve simultaneous mapping and exploration – demonstrating a clear advantage regarding the efficiency of reaching the prompted goal.

The existing zero-shot learning and VLN approaches rely on dedicated sensors to construct a global map on the first run. Subsequent motion decisions are generated by a traditional trajectory planner. Online planning and navigation in dynamic and unknown spaces without a prior map is still an open problem, which we attempt to address in this paper.

3. Rover Master: System Design

We develop a novel robotic platform “*Rover Master*” as a low-power and low-cost UGV platform that is portable and scalable for 2D navigation tasks. The major sensors and actuation components are shown in Fig. 3; it includes a monocular RGB camera and a 2D LiDAR for exteroceptive perception. Four independent wheel assemblies are responsible for actuation; each wheel assembly is modular and self-contained, *i.e.*, it consists of a gearbox, a brushless DC motor, and a suspension system; see Fig. 4b. It also includes a pseudo odometer that uses telemetry data from an electronic speed controller (ESC) which drives the motors. Additionally, the driver stack consists of a flight-controller module originally designed for quad-copters that report onboard sensory data to the host computer for planning and navigation. Unlike existing platforms like the *TurtleBots* [4], *RoverMaster* is designed with an open and spacious chassis to facilitate easy adaptation to any single board computers (SBCs). In our setup, we configured the platform to: **(i)** deliver sufficient computational power to handle a general-purpose vision-language model and other computationally intensive tasks; **(ii)** have enough mechanical stability to hold the camera in an elevated position without excess vibrations even on uneven surfaces; and **(iii)** support 3-DOF motions (forward/backward, sideways and rotation), whereas most existing UGV systems have only 2-DOF (forward surge and twist rotation).

3.1. Task Specific Design for ClipRover

We customize the *Rover Master* platform with a configuration that supports real-time VLN capability for 2D environments. An omnidirectional drive system is chosen to account for the moderate surface irregularities. The four wheels are connected to separate brushless DC motors via a planetary gearbox with a reduction ratio of 16:1. This allows the robot to travel at higher speeds and easily over-

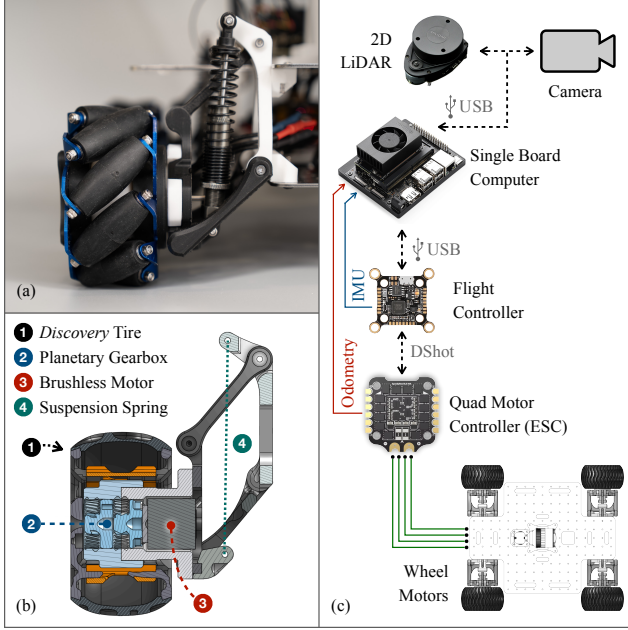


Figure 4. The wheel hub and suspension design are shown on the left: (a) suspension system coupled with the omnidirectional wheel; and (b) cross-section view of the ‘discovery wheel’, in-wheel drive system, and suspension links, assembled and rendered by CAD software. The connection diagram is shown on the right: (c) the dashed line represents physical connection, while solid lines represent logic functions.

come moderate obstacles. A throttle limit of 20% is imposed to ensure operational safety, capping the robot’s maximum speed at approximately 2 m/s. As shown in Fig. 4b, the gearbox and brushless DC motor are integrated into the wheel hub, optimizing the spatial efficiency and smoothness of the drive system. Moreover, the computing pipeline is powered by an Nvidia Jetson Orin module. A FLIR global shutter RGB camera, lifted approximately 30 cm above ground, is used for visual perception. This design ensures that the optical center of the lens aligns with the geometric center of the robot. Besides, the *heading* value from the flight controller’s IMU facilitates 360° scanning capabilities. A 2D LiDAR is mounted at the front of the upper deck as is shown in Fig. 3b. The LiDAR is only used for safety and visualization purposes and does not influence VLN’s decision-making. Further details regarding the LiDAR’s utility are explained in Sec. 5.4.

3.2. Features and Capabilities

One unique advantage of our Rover Master system design is the compactness of its wheels and motor assembly. The four-wheel independent suspension extends its application to uneven surfaces; when using the *Discovery Wheel* (TPU) shown in Fig. 3c and Fig. 4b, it performs well on grasslands, rocky pavements, and even sand (with reduced maneuver-

Table 1. Comparison of *Rover Master* with other standard UGV platforms is shown; the acronyms: [DF] Differential, [OD] Omni-directional, [CFG] Configurable.

Platform	Drive Type	SBC	Onboard Sensors	Add-ons	Est. Cost (USD)
TurtleBot3 (Waffle Pi)	[DF]	RPi4	PiCamera, IMU, LDS laser	Limited	1500
TurtleBot4 (Standard)	[DF]	RPi4	Stereo camera, IMU, RPLiDAR	Limited	2100
<i>Rover Master</i>	[DF] [OD]	[CFG]	RGB camera, IMU, LiDAR	[CFG]	650 850

ability). The suspension system can also be configured to filter out surface bumps and provide better stability for on-board sensors.

The Rover Master platform can be configured to switch between different *drive types* (omnidirectional or differential), *chassis sizes* (with parameterized CAD design), and task-specific *actuation and sensory add-ons* (cameras, LiDARs, manipulators for both indoor and field robotics applications). The chassis plates are designed to house various additional sensors and actuators according to tasks. A comparison of Rover Master with two widely used *TurtleBot* UGV variants is presented in Table 1.

4. ClipRover: Navigation Pipeline

Recent advancements in vision-language models (VLMs) have demonstrated their potential for spatial reasoning and awareness capabilities [10, 14]. Different from traditional approaches, this study explores the feasibility of incorporating VLMs directly into a robot’s autonomy pipeline to facilitate real-time exploration and target identification. To this end, we introduce a modular pipeline that integrates stages for perception, planning, and navigation. The core computational components of the proposed ClipRover navigation pipeline are depicted in Fig. 5.

The proposed pipeline comprises three main stages. The **frontend** processes raw input frames, divides them into tiles, and encodes these tiles into embeddings—numerical vectors representing semantic meanings; In our implementation, the CLIP vision encoder is employed as the frontend. Then, **middlewares** components take the visual embeddings generated by the frontend as input and produce scores that carry specific semantic interpretations. These scores are typically derived by correlating the input embeddings with the middleware’s internal database. The meanings of these scores can vary depending on the application’s requirements. In this study, the middleware generates three types of scores: *navigability*, *familiarity*, and *target confidence*. Lastly, at the **backend**, those scores from middlewares are used to make motion decisions. It is designed to be adaptable, allowing the integration of different algorithms tailored to various applications and environments.

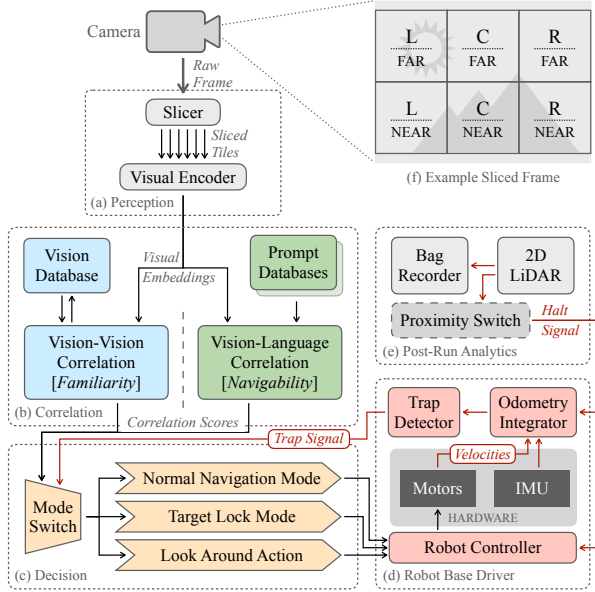


Figure 5. An overview of ClipRover architecture; the *primary* data flow and *supplementary* sensory feedback are in black and red arrows, respectively. The camera frame-slicing strategy is shown in (f); each frame is sliced into two rows (NEAR, FAR) and three columns (LEFT, CENTER, and RIGHT). Each of the six *tiles* is encoded into a separate visual embedding vector for perception.

For this study, a minimal backend was implemented with three operational modes: basic navigation, look-around, and target lock. These modes are dynamically activated or deactivated based on the provided scores.

4.1. Visual Perception Frontend

In the frontend, raw camera frames are sliced into six; the slicing strategies are discussed in Sec. 5.1. Each tile represents a spatial location in robot’s FOV, which are scaled and processed by the CLIP’s visual encoder. As shown in Fig. 5 f, each frame is sliced into $N = 6$ tiles and then re-arranged into a tensor of shape $N \times 3 \times H \times W$, with H and W are the tile height and width in pixels. The encoder processes these inputs and generates an $N \times D$ embedding vector for each tile, where D is the dimensionality of each prediction vector ($D = 512$ in the CLIP model).

Additionally, the standard deviation for each tile is computed and combined with the model’s predictions. This metric serves as an indicator of the *amount of information* present in each tile, proving particularly useful in scenarios where the robot encounters feature-poor, uniformly colored objects such as walls, doors, or furniture. In such instances, an **abnormally** low standard deviation suggests that the vision encoder’s output may lack reliability.

4.2. Navigability Middleware: Vision-Language Correlation

To distinguish navigable spaces from non-navigable ones, we designed a set of *positive prompts* describing clean and navigable environments, such as: “A photo of a (**flat|open|wide|clear**) {**floor|ground|hallway**}”, and a set of *negative prompts* describing spaces that are cluttered by obstacles, such as: “A [**cropped|bad|imcomplete**] photo of a (**blocked|messy|cluttered**) {**scene|space**}” and “A photo of a (**large|way blocking**) {**object|item**}”. As shown in Fig. 6 a, a clear floor is identified as navigable space, while the cluttered scene in Fig. 6 c is accurately categorized as non-navigable.

For target discovery, a similar set of text prompts is used to define the *target* of a task. In our experiments, we use a toy bear (see Fig. 10 b) as the discovery target due to its uniqueness in the scene. We design a set of prompts that describe the target, e.g. “A photo of a (**brown|toy**) {**bear|teddy bear**}”. We also design a set of negative prompts that describe generic objects to filter out false positives, e.g. “A photo of an (**unknown**) {**item|scene|object**}”. As shown in Fig. 6 b, the *target prompt* accurately identified the toy bear, while negative prompts effectively suppressed false positives on unrelated objects, such as the paper box in Fig. 6 c.

The resulting scores for both navigability and target confidence were computed on a per-tile basis. As depicted in Fig. 6 a-c, the CLIP visual encoder generated embeddings for each tile, which were then compared against a prompt database using inner products. The prompt database consisted of pre-encoded text prompts generated by the CLIP text encoder, organized into positive and negative categories. The resulting scores, ranging from -1.0 to 1.0 , were determined by the highest absolute score among the prompt matches.

By employing both positive and negative prompts in each database and selecting the final result based on their contrast, the correlation process becomes more robust against fluctuations in absolute correlation values. This approach is particularly beneficial in environments with varying lighting conditions or complex scenes, where all scores may drift upward or downward depending on the quality of the visual input. Moreover, this method eliminates the need for manually setting a fixed threshold, further enhancing its adaptability.

4.3. Familiarity Middleware: Vision-Vision Correlation

In addition to navigability scores, a *familiarity database* is accumulated in real-time to track previously explored spaces. It is constructed with visual embeddings (512 dimensional vectors) representing known spaces without stor-

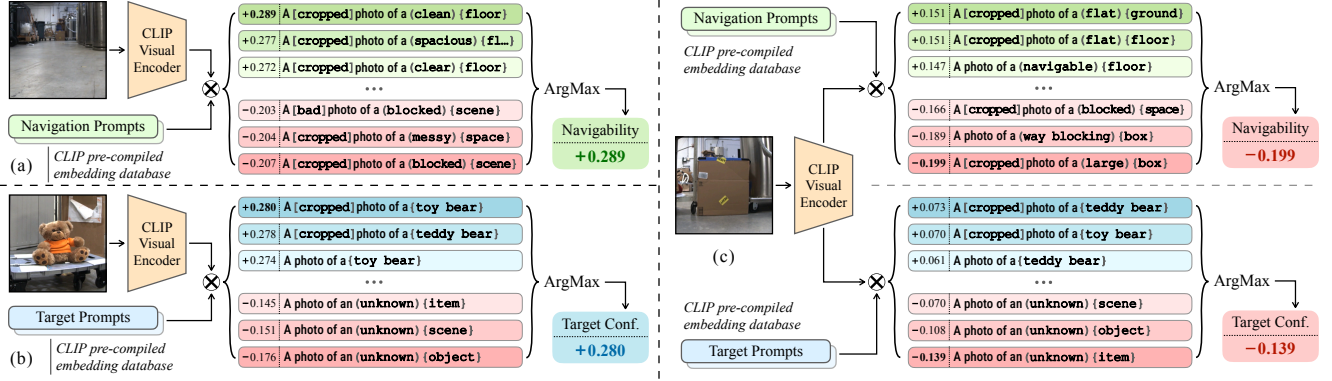


Figure 6. Detailed examples of the proposed *correlation middlewares* are illustrated; the circled cross symbol denotes the inner product of broadcasted vectors. (a) A navigable clean floor is encoded and correlated with the *navigability* database, where green rows (positive prompts) yield higher scores than red rows (negative prompts); the resulting positive final score indicates the space is navigable. (b) A toy bear (the target) is encoded and correlated with the target database, where blue rows (positive prompts) produce higher scores than red rows (negative prompts); the resulting positive final score confirms the target’s presence. (c) A paper box is encoded and correlated with both databases; it corresponds to neither a navigable space nor the target, both scores are negative, indicating the space is not navigable and no target is present. [Best viewed digitally at 2× zoom.]

ing or using actual images. An incoming visual embedding is considered “known” if its correlation score with an existing vector exceeds a predefined threshold. Each new embedding vector is incrementally merged into the familiarity database; we implement the following two strategies for this:

1. Averaging among all vectors that belong to a known point, this involves keeping track of the count of vectors already merged into a known spot (s):

$$v_{\text{next}} = \frac{s}{s+1} \cdot v_{\text{prev}} + \frac{1}{s+1} \cdot v_{\text{new}}$$

2. Performing a rolling average operation upon merging a new vector; this method does not need to keep track of the total count of already merged vectors. Therefore, the vector tends to lean towards newly inserted vectors and gradually “forget” older ones. The “rate of forgetting” can be controlled by a factor λ (a.k.a decay factor):

$$v_{\text{next}} = (1 - \lambda) \cdot v_{\text{prev}} + \lambda \cdot v_{\text{new}}$$

When no *known vector* exists in the database, the incoming vector is inserted as a new data point. Eventually, a familiarity score is generated for each perception vector in the database. This score guides navigation by encouraging the robot to prioritize unexplored areas over revisiting familiar ones.

4.4. Navigation Decision Backend

Lastly, the decision module generates motion commands according to the information provided by the perception and correlation systems. Specifically, a “motion mixer” is introduced as the baseline correlation-to-motion translator. It

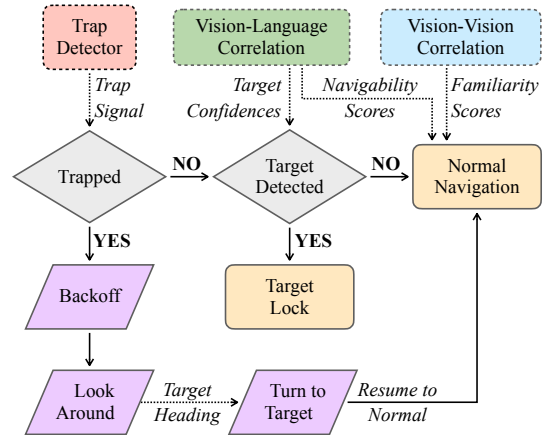


Figure 7. A state diagram illustrating the decision-making process, providing a detailed view of Fig. 5c; blocks with dashed borders are other computational blocks in Fig. 5. Dashed arrows represent data/signal propagation, while solid arrows denote conditions and transitions between states.

takes all aforementioned scores for each tile (*i.e.*, *navigability*, *familiarity*, and *standard deviation*) into consideration and makes an intelligent decision. The motion mixer generally prioritizes highly navigable yet less familiar locations while avoiding areas with minimal texture, indicated by low standard deviation values. To handle non-trivial scenarios, the decision module incorporates two additional functionalities: (1) *trap detection*, enabling the robot to identify and escape from potential dead-ends, and (2) *look-around*, allowing it to reorient itself in complex environments. The overall decision-making process and state transitions are illustrated in Fig. 7.

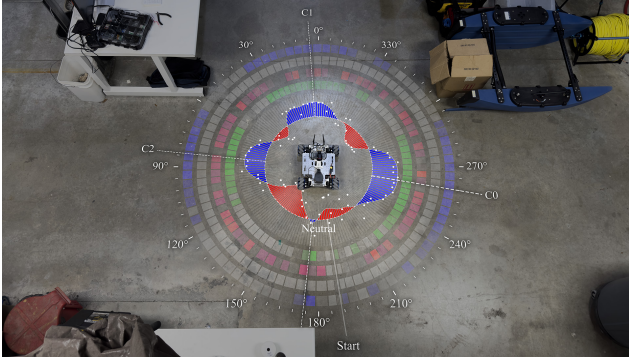


Figure 8. Rendering of a *look around* operation overlaid on a birds-eye view of the robot; it was able to identify navigable paths (blue bars) apart from obstacles (red bars) based on the proposed visual perception pipeline. The candidate headings are annotated as C_i . After the look-around operation, the robot selected C_0 as its next heading according to the area of free space. Details on the color codes and symbols are in Fig. 11.

4.4.1. Trap Detection

In certain scenarios, the robot may encounter a “dead end”, where no navigable path is visible within its FOV. In rare instances, the vision-language model may generate false positive `Nav scores` for scenes it does not adequately comprehend. For example, the lack of salient features can lead to incorrect positive scores when the camera is positioned too close to a plain white wall. Such situations are defined as “trapped” states, which can occur under two conditions: (a) the proximity switch asserts a halt signal for a specified duration, or (b) the cumulative travel distance, as measured by odometry, falls below a defined threshold over a given period. Empirically, the system flags the robot as trapped if it travels less than 0.2 meters within the past 5 seconds.

4.4.2. Look Around

Due to the limited FOV from a single camera, the robot could only see objects in front of it. To address this, a “look around” mechanism (see Fig. 8) is introduced to enable the robot to gain situational awareness by performing a 360° rotation while collecting `Nav scores` associated with different headings. A Gaussian convolution is then applied to these scores to identify the most navigable direction. When recovering from a “trapped” state, the *look around* mechanism prioritizes a direction different from the original heading by a linear factor k , rewarding headings that deviate from the initial orientation. Additionally, a *look around* behavior is triggered at the start of a new mission to ensure the robot identifies the most promising path for exploration.

5. Implementation Details

5.1. Slicing Strategies

To enhance the embedding of positional information within the pipeline, we preprocess the raw camera frames by slicing them into smaller *tiles* before inputting them into the vision-language model. This slicing strategy is specifically designed to optimize the robot’s ability to make informed navigation decisions based on its visual perceptions. As illustrated in Fig. 1, the slicer divides each frame into six (2 rows \times 3 columns) tiles, with the number of horizontal divisions aligned with the robot’s control capabilities. Using smaller tiles instead of the full camera frame reduces visual distractions, thereby improving the accuracy of the correlation results.

The slicing dimensions are consistently maintained across all stages of the pipeline. For instance, under the 2×3 slicing strategy, a frame divided into six tiles produces a corresponding $2 \times 3 \times 512$ matrix of visual embeddings. These embeddings are subsequently aggregated and passed to the correlation middleware, which generates a 2×3 matrix of correlation scores, with each element corresponding to a specific tile. The influence of individual tiles on one another is determined by the logic of the respective correlation middleware. For example, while the familiarity middleware disallows correlations between tiles within the same frame, it may permit correlations between the lower-left tile of a previous frame and the upper-right tile of the current frame.

To preserve spatial context in each tile, sliced regions are slightly expanded beyond their original boundaries. This overlap introduces approximately 20% shared area between adjacent tiles, mitigating the loss of contextual information. This adjustment is beneficial when the camera encounters texture-less surfaces, such as walls, paper boxes, or door panels – where the absence of distinctive features could otherwise impair the robot’s perception and navigation performance.

5.2. Prompt Generation

We also design a prompt system to compose text prompts in a hierarchical template. The proposed design is inspired by WinCLIP [29, 80], an anomaly detection framework. Our prompt system consists of the following templates and notations, which we follow throughout the paper.

- **Top-level prompts** such as:
 - “A [desc.] photo of a (state) {object}”
 - “A [desc.] image of a (state) {object}”
 - “A (state) {object}”
- [descriptions] such as `clear`, `blurry`, `cropped`, `empty`, `corrupted`, *etc.*
- (states) such as `clean`, `clear`, `wide`, `narrow`,

cluttered, messy, way blocking, etc.

- **{objects}** such as **floor, wall, door, object, etc.**

We utilize a YAML-based syntax to define the structure of the prompt databases. YAML, a widely adopted and human-readable markup language, has been extended in our implementation to incorporate additional syntactical features for enhanced flexibility and fine-grained control over the generation of text prompt combinations. Two key features introduced are: Selective integration and in-place expansion.

1. **Selective integration** enables a prompt to bypass certain levels of the template hierarchy, thereby allowing precise customization. For instance, a prompt such as “A **(meaningless)** photo” should not be followed by any **{object}**. This is achieved by terminating the prompt early, omitting the insertion marker (*i.e.* **{}**) in its definition.
2. **In-place expansion** facilitates the collective definition of similar short prompts by using a vertical bar syntax (*i.e.* **|**) to separate terms. This feature is particularly effective when used in conjunction with Selective Integration. For example, the prompt “A photo with no **{context|texture|information}**” is expanded into three distinct prompts, although not fitting into the hierarchical template structure, can be defined as top-level negative prompts, aiding in distinguishing meaningful content from irrelevant or meaningless information.

These enhancements to the YAML-based syntax provide an effective framework for defining and managing prompt databases with high precision and adaptability.

5.3. Performance Optimization

Navigation decisions are a critical component of real-time autonomous robotic systems, requiring rapid execution to ensure safety and operational efficiency. However, most vision-language models are designed as extensions of LLMs, where processing delays and data throughput are less critical. To evaluate the suitability of VLMs for robotic navigation, we identify two key performance metrics:

1. **Decision delay** measures the time elapsed between capturing a frame from the robot’s camera and issuing a corresponding motion command to the motors. This metric reflects the system’s ability to promptly react to environmental changes, such as avoiding obstacles and maintaining safe navigation.
2. **Throughput** quantifies the number of frames processed per second, directly influencing the smoothness of the robot’s motion. Limited computational resources necessitate dropping unprocessed frames, retaining only the latest frame for decision-making. Higher throughput minimizes inter-frame discrepancies, reducing abrupt changes in motion and ensuring smoother transitions.

Mathematically, throughput is the inverse of the decision delay: *i.e.* $f = \frac{1}{T_{\text{delay}}}$.

On the other hand, most robotic systems rely on embedded computers featuring RISC architecture processors and power-limited batteries, prioritizing power efficiency over computational capability. Addressing these constraints, we developed an optimized architecture to maximize resource utilization while improving decision delay and throughput.

Focusing on reducing decision delay and increasing data throughput, our proposed framework divides the navigation pipeline into four major nodes: pre-processing, inference, correlation, and decision-making. Computationally intensive tasks are offloaded to the GPU to exploit parallel processing capabilities. These optimizations were implemented on a power-limited embedded system, balancing efficiency and performance. With the proposed optimizations, we achieve: (i) decision delay: 252.10 ms, an 900% improvement; and (ii) throughput: 5.01 FPS (frames per second), representing a 400% improvement compared to the sequential CPU-based implementation. These results, detailed in Table 2, demonstrate the viability of our VLM-based navigation pipeline for real-time robotic applications under computational constraints.

Table 2. Performance margins of the navigation pipeline of ClipRover at different optimization levels. The acronyms: [**P**] Preprocess, [**I**] Inference, [**C**] Correlation, and [**D**] Decision.

Config.	Mean Data Processing Delay (ms)				Throughput (mean FPS)	
	[P]	[I]	[C]	[D]		Total
CPU Seq.	80.57	2221.67	3.13	0.37	2534.55	0.41 ± 0.07
CPU Para.	73.16	2201.84	3.29	0.40	2463.26	0.44 ± 0.02
GPU Seq.	65.93	178.77	2.94	0.45	327.57	3.22 ± 0.25
GPU Para.	25.32	171.08	3.43	0.48	252.10	5.01 ± 0.36

5.4. Usage of 2D LiDAR

The proposed ClipRover pipeline use only monocular RGB data for VLN navigation decisions. Nevertheless, we installed a 2D 360° scanning LiDAR on the robot for experimental safety, map generation, and comparative analyses. The specific LiDAR functions are listed below.

1. **Emulation of a proximity kill-switch.** The LiDAR serves as a virtual *kill switch* during operation, detecting obstacles in the robot’s intended path. It monitors the motion commands sent to the wheels to infer the robot’s planned trajectory and checks for potential obstructions along that direction. A *halt signal* is asserted upon detection of a potential collision, thus strictly used for safety purposes without influencing the navigation algorithm.
2. **Visualization of map and robot trajectory.** Mapping is performed offline using recorded LiDAR and odometry data, with subsequent trajectory analysis to evaluate navigation efficiency and overall performance. We utilize the *SLAM Toolbox* [49] to generate maps and tra-

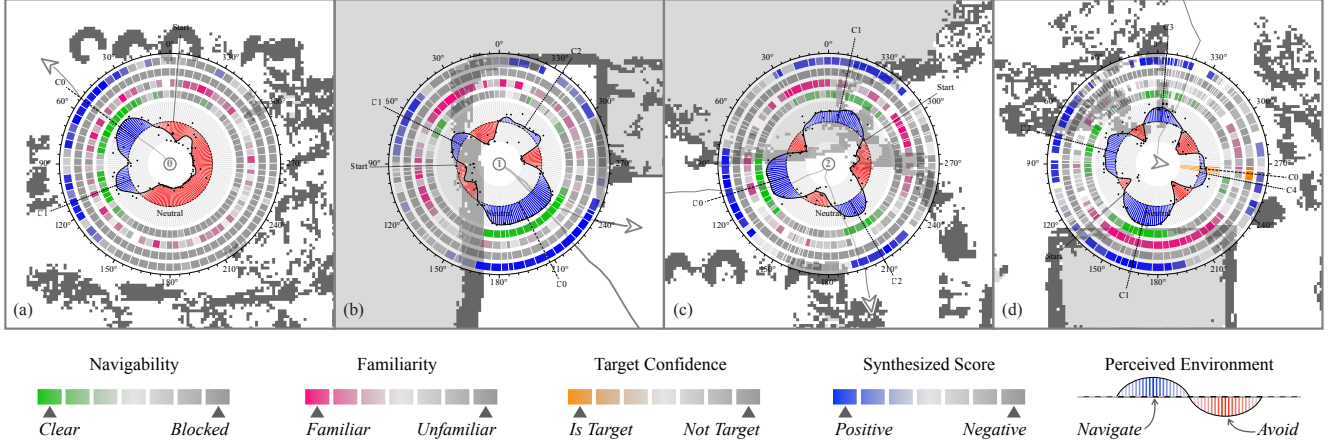


Figure 9. Visualizations of look-around operations during a demonstrative task; candidate directions are depicted as dashed lines (C_i), where candidates with smaller indices are assigned a higher priority. The plots are generated from correlation scores without utilizing additional sensory data. (a) Initial look-around at the center of the map: the system does not incorporate familiarity scores since the familiarity database is uninitialized; thus, the navigability score predominantly influences the robot’s decision. (b) The robot encountered a dead-end and was temporarily trapped; a look-around operation enabled it to identify a navigable path and resume exploration. (c) The robot was trapped due to a false positive navigability perception caused by a transparent object; with a look-around, the system successfully recovered from the false positive and continued its exploration. (d) The target was located nearby in this scenario; through the look-around, the robot was able to identify the target and assign it as the highest-priority candidate. [Best viewed digitally at $2\times$ zoom for clarity.]

jectories, implementing a two-pass process to enhance the quality of the results. In the first pass, the SLAM Toolbox operates in offline mapping mode, creating a high-resolution 2D map of the environment. In the second pass, the pre-constructed map is loaded and run in localization-only mode to generate accurate trajectories using LiDAR localization. Despite this two-pass process, the trajectories generated often exhibit zig-zag patterns caused by a mismatch between SLAM drift correction frequency and the robot’s odometry update rate. These patterns are not observed in the actual motion of the robot, still they affect our performance evaluation due to increased lengths of the projected paths. To mitigate this, we introduce a *stride* parameter to smooth the trajectory. This smoothing parameter reduces the projected trajectory length and better matches the robot’s actual travel distance.

3. **Comparison with simulated algorithms.** A 2D map generated using LiDAR data is employed to simulate and evaluate traditional range sensor-based map traversal and path-planning algorithms for performance comparison. The LiDAR data collected during ClipRover experiments was used to reconstruct the exploration map, which is reused for simulations. This approach ensured that all comparisons were conducted on the same map, providing a fair and consistent evaluation of the different algorithms.

5.5. Wave Front Simulation

We further design a “Wave Front” simulation package to serve as a general baseline metric for comparison between different methods. It utilizes the concept of classic wave function [51] and interprets it as probability distribution, allowing simultaneous exploration of infinity many directions driven by the following equation:

$$\frac{\partial^2}{\partial t^2} \psi(x, y, t) = c^2 \nabla^2 \psi(x, y, t) \quad (1)$$

The simulation implements a 2D Laplacian equation at discretized time steps. Given wave speed c , time step Δt , and spatial step Δx , the wave equation is discretized as:

$$\begin{aligned} \psi(x, y, t_{n+1}) &= 2 \cdot \psi(x, y, t_n) - \psi(x, y, t_{n-1}) \\ &+ \frac{c^2 \Delta t^2}{\Delta x^2} \nabla^2 \psi(x, y, t) \\ \text{s.t. } t_{n+1} - t_n &= \Delta t \end{aligned}$$

Here, the discretized Laplacian operator ∇^2 [67] is defined as:

$$\begin{aligned} \nabla^2 \psi(x, y) &= \psi(x_{i+1}, y_j) + \psi(x_{i-1}, y_j) \\ &+ \psi(x_i, y_{j+1}) + \psi(x_i, y_{j-1}) \\ &- 4 \cdot \psi(x, y) \\ \text{s.t. } x_{i+1} - x_i &= y_{j+1} - y_j = \Delta x \end{aligned}$$

Besides, map boundaries and obstacles are simulated by reflective conditions. That is, at boundary point (x, y) , we

have: $\nabla\psi(x, y) \cdot \hat{\mathbf{n}}_{x,y} = 0$, where $\hat{\mathbf{n}}_{x,y}$ is the normal vector. In a discretized 2D grid, the directions of this normal vector are simplified to four possibilities, *i.e.*, $\hat{\mathbf{n}} \in \{\pm\hat{\mathbf{x}}, \pm\hat{\mathbf{y}}\}$.

To implement the aforementioned boundary condition, the discretized laplacian operator can be rewritten as:

$$\begin{aligned} \nabla^2\psi(x, y) &= k_{i+1,j} \cdot \psi_{i+1,j} + k_{i-1,j} \cdot \psi_{i-1,j} \\ &+ k_{i,j+1} \cdot \psi_{i,j+1} + k_{i,j-1} \cdot \psi_{i,j-1} \\ &- (k_{i+1,j} + k_{i-1,j} + k_{i,j+1} + k_{i,j-1}) \cdot \psi(x, y) \end{aligned}$$

$$s.t. \quad k_{i,j} = \begin{cases} 1 & \text{if } (x_i, y_j) \text{ is free space} \\ 0 & \text{if } (x_i, y_j) \text{ is obstacle} \end{cases}$$

At time $T = 0$, a probability distribution is initialized as a Gaussian distribution centered at the robot’s starting location, with a standard deviation set to half of the robot’s size; the total probability is normalized to 1. At each iteration, the wave function is multiplied by an inverse Gaussian function centered around the target location, effectively reducing the total probability on the map and simulating a draining effect. The simulation terminates when the total remaining probability falls below a defined threshold ($1e^{-4}$ in our experiments). The outcome is a 2D probability distribution $p(t)$ indicating the likelihood of the robot reaching the target at each time step. The mean and standard deviation of this distribution are used for comparison with other trajectory-based algorithms.

At a high level, this algorithm simulates the behavior of infinitely many wall-bouncing robots moving in all possible directions. Notably, the drain operation creates a uniform gradient toward the target, subtly guiding the robot. As a result, the algorithm performs slightly better than a purely randomized wall-bouncing simulation, which lacks any target information. The travel distance when the first non-zero probability is detected is used as the baseline distance for each origin-target combination. For relative performance comparisons, as shown earlier in Fig. 2, the travel distances are normalized by this baseline distance before aggregating the results.

6. Experimental Analyses

6.1. Experiment Setup

Real-world experiments were conducted in an indoor workspace, as depicted in Fig. 10 a. This environment was selected for its cluttered layout and complex details, which include numerous obstacles, potential traps, and loops, providing a challenging setting for comprehensive analysis. As shown in Fig. 10, the robot was tasked with exploring the lab space while searching for a designated target—a toy bear approximately 20 cm tall and 10 cm wide, chosen for its distinctive appearance within the test scene. For each task, the source (robot’s starting position) and destination (target lo-

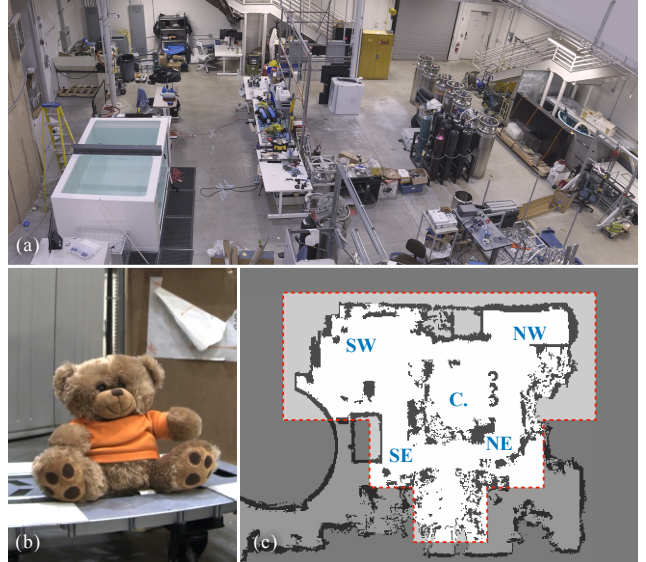


Figure 10. The environment used for real world exploration and discovery experiments: (a) An overview of the machine hall. (b) A photo of a toy bear that is used as the *discovery target*. (c) A 2D map of the experimental space, with major corner locations annotated in blue; the area utilized for the experiments is enclosed within the dashed red line.

cation) were selected from five predefined regions (*e.g.*, SW, C, NW, NE, SE), as labeled in Fig. 10 c.

6.2. Performance Evaluation

Evaluation criteria. Our experimental trials are designed to evaluate *efficiency* of exploring an area and *success rates* of finding a target with no prior map or knowledge about the target. To quantify these, we use the total distance traveled (trajectory length) before approaching the target as the core metric. Instead of the total duration of the task, the travel distance metric is agnostic to the CPU/GPU performance of the onboard computer and the capability of the mechanical driving system, which are considered external factors that can be improved independently.

Algorithms for comparison. We compare the performance of the proposed **ClipRover** system with six widely used map-traversal and path-finding algorithms. For fair comparisons, a novel 2D simulation framework, **RoboSim2D**, is developed. It utilizes 2D LiDAR maps generated from recorded scans of the same environment used in real-world experiments. Additionally, the size of the simulated robot was configured to match the dimensions of the physical robot, ensuring consistency across simulations and the real platform.

For map traversal algorithms [56], we consider:

1. **Random Walk:** Starts with a given heading, then randomly selects a new heading when an obstacle is encountered.

2. **Wall Bounce:** Starts at a given heading, then bounces off obstacles based on the normal vector of the impact point.
3. **Wave Front:** Starts as a Gaussian probability distribution, then spreads outwards and bounces off obstacles. A detailed explanation is in Sec. 5.5.

Additionally, we compare the following Bug Algorithms [45, 47]:

1. **Bug0:** Moves straight toward the target until encountering an obstacle, then follows the obstacle boundary until it can resume a direct path to the target.
2. **Bug1:** Heads towards the target when possible, otherwise, circumnavigates the obstacle. After looping an obstacle, travels to the point with the minimum distance on the loop.
3. **Bug2:** Circumnavigates obstacles upon encountering until it crosses the direct line from the start to the target (the `m-line`), then resumes a straight path toward the target.

Criteria of failure. Due to practical limitations, a mission is considered a failure if the distance traveled exceeds a predefined upper limit. For real-world experiments conducted in the test area (approximately 12×16 m), this limit is set to 100 meters. In simulations, the limit is set to 1,000 meters for random walk, wall-bouncing, and wave-front algorithms. For Bug algorithms, loop detection is employed to identify endless loops, which are classified as mission failures. Since failed missions yield infinite travel distances, they are excluded from the metrics presented in Table 3. Instead, they are reported separately in the overall performance Table 4 and visualized in the relative performance plot in Fig. 2.

Evaluation metrics. As observed in our simulation results, for a given amount of information, the success rate R is inversely proportional to the normalized path length L . This relationship is expressed by a commonly adopted performance metric for VLN systems, known as *Success weighted by Path Length* (SPL) [5], defined as:

$$\text{SPL} = \frac{1}{N} \sum_{i=1}^N S_i \frac{l_i}{\max(p_i, l_i)}. \quad (2)$$

Note that, for each source-target combination, the first contact distance of WaveFront simulation is used as the baseline distance D_{baseline} . With the choice of $l = D_{\text{baseline}}$, we have $p_i > l, \forall p_i \in \{p\}$; hence, the above equation is simplified to:

$$\text{SPL} = \frac{1}{N} \sum_i^{S_i=1} \frac{D_{\text{baseline}}}{p_i} = \frac{N_s}{N} \sum_i^{S_i=1} \frac{L_i}{N_s} = R \cdot \bar{L} \quad (3)$$

$$\text{s.t.} \begin{cases} L_i = \frac{D_{\text{baseline}}}{p_i} & - \text{Inverse Relative Distance} \\ N_s = \sum_i^{S_i=1} 1 & - \text{Number of Success Runs} \\ R = \frac{N_s}{N} & - \text{Success Rate} \\ \bar{L} = \sum_i^{S_i=1} \frac{L_i}{N_s} & - \text{Mean Inverse Path Length} \end{cases} \quad (4)$$

As a consequence, the SPL metric equates to an inverse proportional relation between two quantities, namely the success rate R and the mean inverse path length \bar{L} , as follows:

$$\bar{L} = \frac{\text{SPL}}{R}. \quad (5)$$

However, experimental data reveal that the curvature of the SPL function does not align well with the observed R - \bar{L} curve shown in Fig. 2. To better model the observed data, **we introduce a new metric** ε to represent the amount of information available to a given algorithm. It has a range of $[0, 1]$. When $\varepsilon = 0$, the algorithm operates without environmental information and lacks sensing capabilities beyond collision detection, as seen in methods like random walk and wall bounce. As ε approaches 1, it gains more information or has higher environment sensing capability, and the performance is expected to increase accordingly. Considering the impact of ε , the revised relationship reduces to:

$$\bar{L} = \frac{\varepsilon'}{(kR + t)^\beta} \quad (6)$$

$$\text{s.t. } \beta = \alpha \cdot \varepsilon' \text{ and } \varepsilon' = 1 + \omega \cdot \varepsilon \quad (7)$$

where k , t , and α are hyper-parameters specific to the environment. They are derived using linear regression with $\varepsilon = 0$; additionally, ω is solvable by setting $\varepsilon = \bar{L} = R = 1$.

6.3. Qualitative and Quantitative Analyses

We conduct extensive real-world experiments with over 60 trials based on various combinations of source-target locations shown in Fig. 10. For the proposed ClipRover system, three trials were performed for each origin-target pair. In comparison, 200 trials were recorded for each random walk experiment, while 180 evenly distributed headings were recorded for each combination of the wall bounce runs.

Samples of the trajectories traversed by ClipRover and other algorithms are presented in Fig. 11, overlaid on a 2D map of the environment. Under *normal navigation mode*, ClipRover exhibits a human-like motion strategy by navigating near the center of open spaces, enhancing exploration efficiency, and reducing the likelihood of becoming trapped by obstacles. In contrast, path-finding algorithms often follow the contours of obstacles due to their lack of semantic scene understanding. During *look-around operations* (see Fig. 8 and Fig. 9), ClipRover accurately discriminates between navigable spaces and obstacles. Additionally, it demonstrates a preference for unexplored (unfamiliar) areas

Table 3. Quantitative performance comparison of the exploration (random walk, wall bounce, and wavefront) and path-finding (Bug 0/1/2) algorithms in terms of trajectory length. All units are in meters; see Fig. 10 for the source-target layouts. The acronyms: [L] and [R] represent left and right turn rules, respectively; the failure cases are shown as ‘×’ markers.

Task Setup		ClipRover ★	Random Walk	Wall Bounce	Wave Front	Bug0		Bug1		Bug2	
Source	Target	Avg. ± Std.	Avg. ± Std.	Avg. ± Std.	Avg. ± Std.	[L]	[R]	[L]	[R]	[L]	[R]
C.	N.W.	8.3± 2.1	149.6±18.6	169.3±14.9	162.7±55.8	5.9	×	75.8	42.2	6.0	×
	N.E.	27.2± 2.7	326.5±27.0	313.1±19.4	247.4±74.3	×	×	63.0	49.5	13.4	×
	S.W.	29.0± 7.1	256.7±19.4	233.4±15.6	236.9±66.8	×	7.9	43.7	72.5	×	8.6
	S.E.	27.0± 3.7	370.6±23.4	338.4±18.8	285.2±82.5	×	×	54.9	59.2	23.2	19.4
N.W.	C.	21.6±10.9	233.3±26.0	193.6±16.2	192.2±55.8	×	5.9	47.0	67.7	40.1	6.0
	N.E.	8.7± 2.2	253.7±25.4	220.1±18.3	233.5±61.0	7.4	7.4	7.4	7.4	7.4	7.4
	S.W.	9.9± 0.0	290.2±21.7	241.5±14.6	239.4±69.0	9.6	×	132.1	84.4	10.0	×
	S.E.	29.6±17.9	338.8±24.9	332.7±19.9	281.5±78.7	14.8	×	63.8	52.0	15.7	24.8
N.E.	C.	23.6±12.1	275.6±24.5	251.2±20.0	223.4±62.6	×	9.2	50.5	60.9	28.0	12.0
	N.W.	9.1± 2.4	157.5±21.5	187.0±17.0	181.9±45.6	6.9	×	6.9	75.7	6.9	×
	S.W.	42.0± 9.5	236.2±19.3	250.9±14.2	237.9±70.5	14.3	13.9	58.9	55.2	17.1	24.0
	S.E.	48.7±19.4	235.8±22.5	277.9±18.2	240.1±67.9	7.6	×	68.3	44.7	7.7	41.0
S.W.	C.	19.3± 6.0	340.9±26.8	331.7±19.1	266.0±66.2	×	×	66.1	50.0	12.0	33.7
	N.W.	15.9± 4.5	329.3±22.6	330.6±17.2	259.9±63.8	×	10.5	65.1	19.7	×	10.9
	N.E.	31.1± 3.1	396.7±29.0	288.3±16.7	276.8±78.6	×	×	51.8	65.1	27.5	15.8
	S.E.	31.8±11.2	217.2±22.0	208.3±16.5	220.7±62.3	7.8	×	10.1	71.4	8.0	×
S.E.	C.	29.7± 8.0	386.0±25.9	311.1±17.7	283.3±72.9	×	16.1	57.2	54.5	18.2	21.2
	N.W.	22.5± 4.4	369.9±26.5	298.7±17.7	262.8±63.5	×	×	50.6	64.9	25.5	15.1
	N.E.	5.7± 0.2	302.3±28.8	279.7±20.1	249.3±60.8	6.1	×	6.1	73.4	6.1	×
	S.W.	11.1± 1.8	156.3±20.4	147.2±13.2	171.3±58.7	7.5	7.5	7.5	7.5	7.5	7.5

Table 4. Quantitative performance of ClipRover and other algorithms in comparison. Metrics used are defined in Eq. 4.

Method	Success Rate	Mean Inverse Path Length	Additional Requirements
ClipRover ★	95.00%	2.66± 1.73	
Random Walk	50.00%	10.77± 6.26	
	80.00%	20.56±14.65	
Wall Bounce	50.00%	9.58± 5.58	None
	80.00%	18.71±13.66	
Wave Front	50.00%	13.86± 5.31	
	80.00%	27.30±10.11	
Bug0	45.00%	1.14± 0.08	Target location
Bug1	100.00%	6.34± 3.98	Target location, Memory of trajectory
Bug2	80.00%	1.90± 1.51	Target Location, m-line Detection

over previously visited (familiar) regions, contributing to improved efficiency compared to traditional map-traversal algorithms.

Out of all 60 trials, 3 failure cases were recorded, yielding 95% overall success rate for ClipRover. Among them, two were caused by the trajectory length exceeding the up-

per limit, while the other one was caused by the robot getting jammed by a reflective metal tank, which was not detected by either the VLN pipeline or the LiDAR proximity switch.

The quantitative results categorized by source and target locations are presented in Table 3. To ensure comparability across different source-target pairs, the travel distance for each row is normalized by the baseline travel distance and then aggregated into Table 4. For randomized algorithms, the success rate R is a configurable hyperparameter. Sample results for $R = 50\%$ and $R = 80\%$ are provided to represent their underlying performance in Table 4, with the corresponding equipotential curves previously shown in Fig. 2. In contrast, deterministic algorithms (such as Bug variants) have a fixed success rate. Their performances are reported directly in Table 4 and visualized in Fig. 2 for comparison.

As these results demonstrate, ClipRover averages $2.66 \times D_{\text{baseline}}$ travel distance before reaching the target, while the next best score is from Wall Bounce, with $9.58 \times D_{\text{baseline}}$ at a significantly lower success rate (50%). Note that, it achieves this performance gains despite having the same prior information as the map traversal algorithms. On the

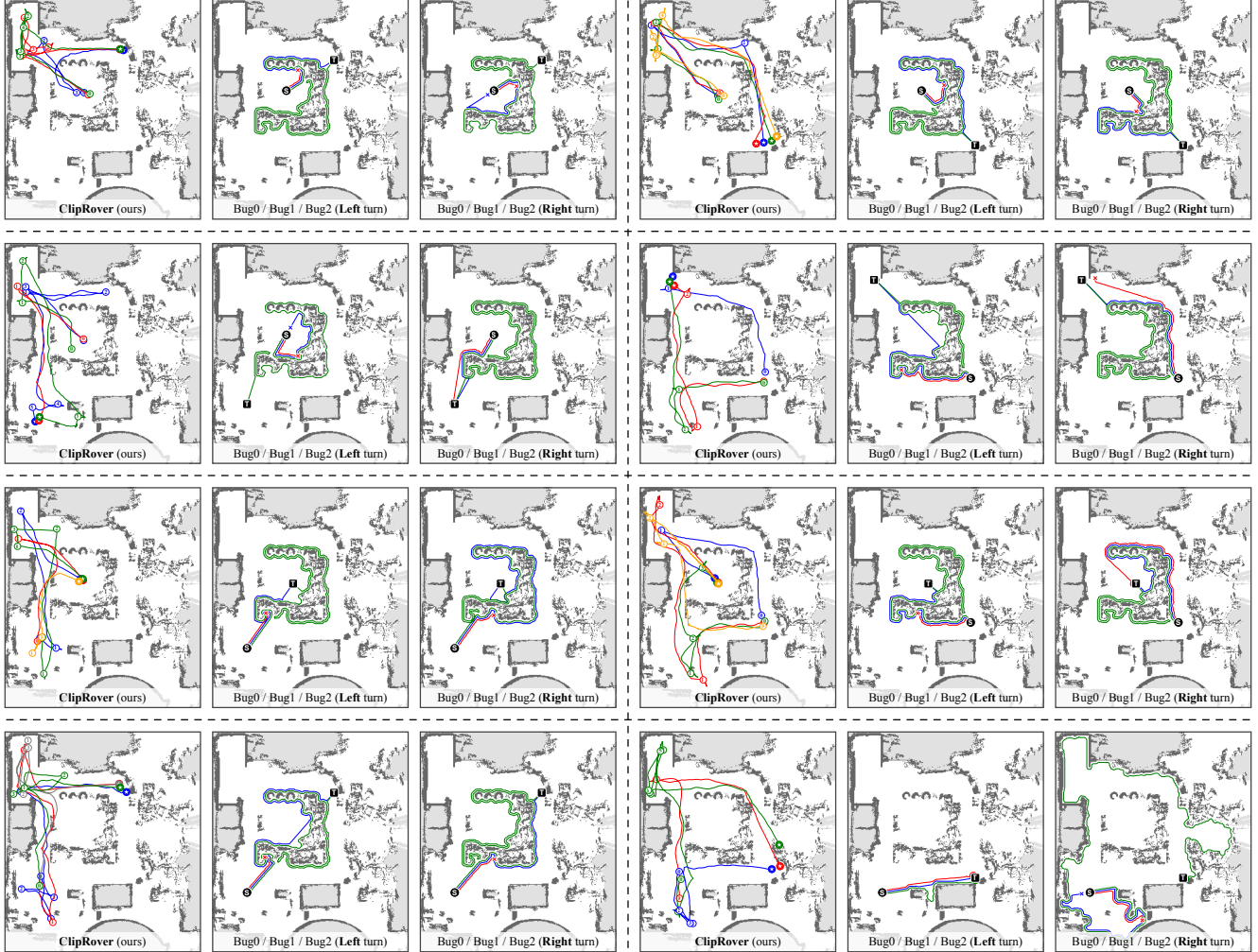


Figure 11. Sample results of autonomous exploration and target discovery by ClipRover compared to Bug algorithms. The trajectories of each algorithm are overlaid on a 2D map of the test environment. Circled numbers indicate the *look around* operations of ClipRover and the corresponding waypoints sequence it followed. For Bug algorithms, the red, green, and blue trajectories represent paths traversed by *Bug0*, *Bug1*, and *Bug2*, respectively. Best viewed digitally at $2\times$ zoom for clarity; more results are in the Appendix. A video demonstration is provided here: <https://youtu.be/84XLM-GbhS8>.

other hand, although the Bug* algorithms uses additional information about the environment map and target location, ClipRover (95%) still outperforms Bug1 ($6.34 \times D_{\text{baseline}}$) by trajectory lengths, and offers significantly higher success rates than Bug0 (45%) and Bug2 (80%) algorithms.

In summary, the proposed system outperforms traditional map traversal algorithms by significant margins in both success rate and trajectory efficiency, given the same amount of information. Despite the inherent disadvantage of operating without prior target knowledge or precise localization, the system achieves performance comparable to path-finding algorithms. Notably, in many scenarios, it surpasses path-finding algorithms in either trajectory efficiency or success rates. These results highlight the effectiveness of

the proposed pipeline for simultaneous exploration and target discovery tasks.

6.4. Comparative Analyses of SOTA VLNs

We also compare ClipRover with state-of-the-art VLN systems based on their features and prerequisites. The characteristics of each system are summarized in Table 5. Compared to existing systems, ClipRover uniquely requires zero prior knowledge of the task space and operates solely with monocular RGB perception. Additionally, contemporary VLN systems do not directly produce low-level motion commands but instead generate high-level instructions that depend on another traditional localization and navigation pipeline for the eventual motion execution. In contrast, ClipRover directly outputs low-level motion commands,

Table 5. A qualitative comparison of features and prerequisites among state-of-the-art VLN systems.

VLN System	Focus	Prerequisites	Sensing Modality	Output Type	Deployment	Evaluation
CLIP-Nav [14]	Scene	Pre-captured Images of candidate locations	N/A	Choice of an Image for Next Step	Simulation	Success rate (relative)
CLIP on Wheels [17]	Object	Unspecified	RGB-D Camera	Revalance map of the current View	Simulation	Accuracy & Path length
SEEK [19]	Object	Pre-built dynamic scene graph and relational semantic network	LiDAR, 3 RGB Cameras Real-time SLAM	Sequence of Waypoints	Real World	Success rate & Path length
GCN for Navigation [36]	Object	Pre-constructed knowledge graph of object relations	Monocular RGB Camera	Choice of a Pre-encoded Action	Simulation	Path length & Success rate
Chen <i>et al.</i> [11]	Scene	Pre-constructed node graph of navigable space	N/A	Choice of Next Node	Simulation	Success rate & Completion Rate
ClipRover ★	Hybrid	None	Monocular RGB Camera	Direct Motion Commands (3 _{DOF})	Real World	Path length & Success rate

eliminating the need for auxiliary control and localization systems. This feature makes ClipRover particularly suitable for rapid deployment on low-cost robots with limited computational and sensing resources.

It is important to note that, although the calculation of the bare SPL metric (Eq. 2) for ClipRover is possible, it is infeasible to conduct a fair quantitative comparison against the aforementioned systems. For example, SEEK [19] reported $65 \pm 35\%$ SPL for random walk, while our random walk simulation yielded $8.4 \pm 11\%$ SPL, showing a magnitude of difference. Preliminary analysis suggests that this discrepancy stems from SEEK’s reliance on a node-graph map structure, which reduces the problem space to a finite set of graph nodes and edges. In contrast, ClipRover operates continuously in an unknown environment, resulting in a substantially larger problem space facilitating active robot navigation with no prior information or pre-compiled knowledge graphs.

7. Limitations, Failure Cases, and Potential Improvements of ClipRover

7.1. Texture-less or Transparent Surfaces

As a vision-driven system, the proposed ClipRover pipeline encounters challenges in environments with texture-less or transparent surfaces. When presented with a blank or non-informative image, the inherent VLM struggles to generate meaningful responses, disrupting the entire pipeline. For instance, as demonstrated in Fig. 9 d (C1), the robot mistakenly classified a water tank with transparent walls as navigable space. This error occurred because the VLM perceived the interior of the tank, visible through its transparent walls, as accessible terrain. To mitigate this issue, a standard deviation threshold was introduced to filter out ambiguous tiles. While this approach improved performance, the system still exhibits a general tendency to misclassify transparent or uniformly colored surfaces, such as blank walls or white floors, as navigable space. These challenges persist, partic-

ularly when the robot is positioned close to such surfaces, where the lack of texture further confuses the VLM. Note that this issue with transparent and texture-less walls has been an open problem for 2D indoor navigation by mobile robots [78].

7.2. Open Space and Artificially Constructed Mazes

The system’s reliance on the semantic understanding capabilities of the VLM limits its effectiveness in large, open spaces. Without sufficient visual cues or meaningful objects in the environment, the robot cannot optimize its exploration based on semantic information. In such cases, the robot defaults to moving straight ahead until it encounters visually significant objects, such as obstacles, at which point its correlation middleware resumes providing meaningful guidance. This limitation reduces the system’s efficiency in environments devoid of distinguishing visual features.

Moreover, our experiments in artificially constructed mazes, such as those built from paper boxes, revealed limitations in the VLM’s ability to differentiate between the maze walls such as monochrome cardboards, and floors. As a result, the robot either failed to navigate or attempted to collide with the maze walls. This behavior can be attributed to the lack of similar examples in the VLM’s training data, which likely did not include artificially constructed environments of this nature. Consequently, the system is better suited to real-world scenarios where the VLM has been trained on relevant, diverse visual data. This observation suggests that our proposed system will work most effectively in real-world environments where VLMs generally work well.

7.3. Familiarity Saturation

The *familiarity* middleware is designed to help the robot avoid revisiting already explored areas by accumulating memory of the environment. However, during extended missions, the familiarity database tends to saturate due to the repetitive nature of objects in the environment. Once all

unique objects are recorded, the system struggles to prioritize unexplored areas effectively. Future iterations of the system could implement a memory decay mechanism, allowing older entries in the familiarity database to fade over time, thereby prioritizing new observations and maintaining exploration efficiency.

7.4. Adaptive Slicing Strategies

In our current implementation of ClipRover, a fixed slicing strategy is used based on the camera frame’s aspect ratio, which generally performs well in general. However, in specific scenarios involving narrow navigable spaces (*e.g.*, a 50 cm gap between two obstacles), the robot often fails to recognize these spaces as traversable. This is because the narrow passage does not occupy an entire tile, leaving obstacles visible in all tiles and leading the system to avoid the space rather than navigate through it. Future improvements could include the development of advanced slicing strategies that dynamically adapt the region of interest (ROI) based on the surrounding environment. This could be achieved using sparse object detection (bounding box) or pixel-wise segmentation models, enabling better handling of narrow spaces.

7.5. High-Level Reasoning and Task Narration

One of the most promising extensions of this work lies in incorporating high-level reasoning and task narration using an integrated LLM. With this addition, the robot could leverage common-sense reasoning to make more intelligent navigation decisions. For example, when prompted to locate an item in a different room, the robot could infer that heading toward a door is the most logical action. Moreover, in bandwidth-limited applications, the LLM could provide real-time task narration by interpreting visual embeddings to describe mission progress. This approach would significantly reduce the communication bandwidth required compared to streaming raw video. While the architecture lays the foundation for these enhancements, their implementation remains a future work. By addressing these limitations and pursuing the outlined improvements, ClipRover can evolve into a more robust, efficient, and versatile platform for VLN in complex real-world environments.

8. Conclusion

In this paper, we introduced **ClipRover**, a novel navigation pipeline designed for simultaneous exploration and target discovery by autonomous ground robots in unknown environments, leveraging the power of VLMs. Unlike traditional approaches that decouple exploration from path planning and rely on inefficient algorithms, ClipRover enables **zero-shot inference** and efficient navigation using only monocular vision, without prior maps or target-specific information. To validate our approach, we developed a

functional prototype UGV platform named **Rover Master**, optimized for general-purpose VLN tasks in real-world environments. Extensive evaluations demonstrated that ClipRover outperforms state-of-the-art map traversal algorithms in efficiency and achieves comparable performance to path-planning methods that rely on prior knowledge. The integration of a CLIP-based VLM into a real-time navigation system underscores the potential of ClipRover to advance intelligent robotic exploration. As a modular and flexible framework, ClipRover lays the groundwork for future research in applying VLMs to more complex and dynamic robotic applications such as autonomous warehousing, security patrolling, and smart home assistance.

Acknowledgments

This work is supported in part by the National Science Foundation (NSF) grants #2330416, #19244; the Office of Naval Research (ONR) grants #N000142312429, #N000142312363; and the University of Florida (UF) ROSF research grant #132763.

References

- [1] Adnan Abdullah, Titon Barua, Reagan Tibbetts, Zijie Chen, Md Jahidul Islam, and Ioannis Rekleitis. CaveSeg: Deep Semantic Segmentation and Scene Parsing for Autonomous Underwater Cave Exploration. In *IEEE International Conference on Robotics and Automation (ICRA)*. IEEE, 2024.
- [2] Khalid Al-Mutib, Mansour AlSulaiman, Muhammad Emaduddin, Hedjar Ramdane, and Ebrahim Mattar. D* lite based real-time multi-agent path planning in dynamic environments. In *2011 third international conference on computational intelligence, modelling & simulation*, pages 170–174. IEEE, 2011.
- [3] Francesco Amigoni and Vincenzo Caglioti. An information-based exploration strategy for environment mapping with mobile robots. *Robotics and Autonomous Systems*, 58(5): 684–699, 2010.
- [4] Robin Amsters and Peter Slaets. *Turtlebot 3 as a Robotics Education Platform*, pages 170–181. 01 2020. ISBN 978-3-030-26944-9. doi: 10.1007/978-3-030-26945-6-16.
- [5] Peter Anderson, Angel X. Chang, Devendra Singh Chaplot, Alexey Dosovitskiy, Saurabh Gupta, Vladlen Koltun, Jana Kosecka, Jitendra Malik, Roozbeh Mottaghi, Manolis Savva, and Amir R. Zamir. On evaluation of embodied navigation agents. *CoRR*, abs/1807.06757, 2018. URL <http://arxiv.org/abs/1807.06757>.
- [6] Peter Anderson, Qi Wu, Damien Teney, Jake Bruce, Mark Johnson, Niko Sünderhauf, Ian Reid, Stephen Gould, and Anton van den Hengel. Vision-and-language navigation: Interpreting visually-grounded navigation instructions in real environments, 2018. URL <https://arxiv.org/abs/1711.07280>.
- [7] Rodrigue Bonnevie, Daniel Duberg, and Patric Jensfelt. Long-term exploration in unknown dynamic environments. In *2021 7th International Conference on Automation*,

- Robotics and Applications (ICARA)*, pages 32–37. IEEE, 2021.
- [8] Norlida Buniyamin, W Wan Ngah, Nohaidda Sariff, Zainuddin Mohamad, et al. A simple local path planning algorithm for autonomous mobile robots. *International journal of systems applications, Engineering & development*, 5(2): 151–159, 2011.
- [9] Ade Candra, Mohammad Andri Budiman, and Kevin Hartanto. Dijkstra’s and a-star in finding the shortest path: A tutorial. In *2020 International Conference on Data Science, Artificial Intelligence, and Business Analytics (DATABIA)*, pages 28–32. IEEE, 2020.
- [10] Boyuan Chen, Zhuo Xu, Sean Kirmani, Brain Ichter, Dorsa Sadigh, Leonidas Guibas, and Fei Xia. Spatialvlm: Endowing vision-language models with spatial reasoning capabilities. In *Proceedings of the IEEE/CVF Conference on Computer Vision and Pattern Recognition*, pages 14455–14465, 2024.
- [11] Kevin Chen, Juan Pablo de Vicente, Gabriel Sepulveda, Fei Xia, Alvaro Soto, Marynel Vazquez, and Silvio Savarese. A behavioral approach to visual navigation with graph localization networks. In *Proceedings of Robotics: Science and Systems, Freiburg/Breisgau, Germany, June 2019*. doi: 10.15607/RSS.2019.XV.010.
- [12] Thomas H Cormen, Charles E Leiserson, Ronald L Rivest, and Clifford Stein. *Introduction to algorithms*. MIT press, 2022.
- [13] Subir Kumar Das, Kousik Roy, Tanmay Pandey, Aniket Kumar, Ajoy Kumar Dutta, and Subir Kumar Debnath. Modified critical point—a bug algorithm for path planning and obstacle avoiding of mobile robot. In *2020 International Conference on Communication and Signal Processing (ICCSP)*, pages 351–356. IEEE, 2020.
- [14] Vishnu Sashank Dorbala, Gunnar Sigurdsson, Robinson Piramuthu, Jesse Thomason, and Gaurav S Sukhatme. CLIPnav: Using CLIP for zero-shot vision-and-language navigation. In *Workshop on Language and Robotics at CoRL 2022*, 2022.
- [15] Dave Ferguson and Anthony Stentz. Using interpolation to improve path planning: The field d^* algorithm. *Journal of Field Robotics*, 23(2):79–101, 2006.
- [16] Matthew Gadd and Paul Newman. A framework for infrastructure-free warehouse navigation. In *2015 IEEE International Conference on Robotics and Automation (ICRA)*, pages 3271–3278. IEEE, 2015.
- [17] Samir Yitzhak Gadre, Mitchell Wortsman, Gabriel Ilharco, Ludwig Schmidt, and Shuran Song. Cows on pasture: Baselines and benchmarks for language-driven zero-shot object navigation. *2023 IEEE/CVF Conference on Computer Vision and Pattern Recognition (CVPR)*, pages 23171–23181, 2022. URL <https://api.semanticscholar.org/CorpusID:254636632>.
- [18] Samir Yitzhak Gadre, Mitchell Wortsman, Gabriel Ilharco, Ludwig Schmidt, and Shuran Song. Clip on wheels: Zero-shot object navigation as object localization and exploration. *arXiv preprint arXiv:2203.10421*, 3(4):7, 2022.
- [19] Muhammad Fadhil Ginting, Sung-Kyun Kim, David D. Fan, Matteo Palieri, Mykel J. Kochenderfer, and Ali akbar Aghamohammadi. SEEK: Semantic reasoning for object goal navigation in real world inspection tasks. In *Proc. of Robotics: Science and Systems*, 2024.
- [20] Tianrui Guan, Yurou Yang, Harry Cheng, Muyuan Lin, Richard Kim, Rajasimman Madhivanan, Arnie Sen, and Dinesh Manocha. Loc-zson: Language-driven object-centric zero-shot object retrieval and navigation. *ArXiv*, abs/2405.05363, 2024. URL <https://api.semanticscholar.org/CorpusID:269635354>.
- [21] KR Guruprasad. Egressbug: a real time path planning algorithm for a mobile robot in an unknown environment. In *Advanced Computing, Networking and Security: International Conference, ADCONS 2011, Surathkal, India, December 16-18, 2011, Revised Selected Papers*, pages 228–236. Springer, 2012.
- [22] Peter E Hart, Nils J Nilsson, and Bertram Raphael. A formal basis for the heuristic determination of minimum cost paths. *IEEE transactions on Systems Science and Cybernetics*, 4(2):100–107, 1968.
- [23] Kazi Mahmud Hasan, Khondker Jahid Reza, et al. Path planning algorithm development for autonomous vacuum cleaner robots. In *2014 International Conference on Informatics, Electronics & Vision (ICIEV)*, pages 1–6. IEEE, 2014.
- [24] Carlos Alberto Velásquez Hernández and Flavio Augusto Prieto Ortiz. A real-time map merging strategy for robust collaborative reconstruction of unknown environments. *Expert Systems with Applications*, 145:113109, 2020.
- [25] Chenguang Huang, Oier Mees, Andy Zeng, and Wolfram Burgard. Visual language maps for robot navigation. In *2023 IEEE International Conference on Robotics and Automation (ICRA)*, pages 10608–10615. IEEE, 2023.
- [26] Galadrielle Humblot-Renaux, Letizia Marchegiani, Thomas B Moeslund, and Rikke Gade. Navigation-oriented scene understanding for robotic autonomy: Learning to segment driveability in egocentric images. *IEEE Robotics and Automation Letters*, 7(2):2913–2920, 2022.
- [27] Gabriel Ilharco, Mitchell Wortsman, Ross Wightman, Cade Gordon, Nicholas Carlini, Rohan Taori, Achal Dave, Vaishaal Shankar, Hongseok Namkoong, John Miller, Hannaneh Hajishirzi, Ali Farhadi, and Ludwig Schmidt. Openclip, July 2021. URL <https://doi.org/10.5281/zenodo.5143773>. If you use this software, please cite it as below.
- [28] Md Jahidul Islam, Jungseok Hong, and Junaed Sattar. Person-following by Autonomous Robots: A Categorical Overview. *The International Journal of Robotics Research (IJRR)*, 38(14):1581–1618, 2019. doi: 10.1177/0278364919881683.
- [29] Jongheon Jeong, Yang Zou, Taewan Kim, Dongqing Zhang, Avinash Ravichandran, and Onkar Dabeer. Winclip: Zero/few-shot anomaly classification and segmentation. In *Proceedings of the IEEE/CVF Conference on Computer Vision and Pattern Recognition (CVPR)*, pages 19606–19616, June 2023.
- [30] Ishay Kamon and Ehud Rivlin. Sensory-based motion planning with global proofs. *IEEE transactions on Robotics and Automation*, 13(6):814–822, 1997.

- [31] Ishay Kamon, Ehud Rivlin, and Elon Rimon. A new range-sensor based globally convergent navigation algorithm for mobile robots. In *Proceedings of IEEE International Conference on Robotics and Automation*, volume 1, pages 429–435. IEEE, 1996.
- [32] Sertac Karaman and Emilio Frazzoli. Sampling-based algorithms for optimal motion planning. *The international journal of robotics research*, 30(7):846–894, 2011.
- [33] Lydia E Kavraki, Mihail N Kolountzakis, and J-C Latombe. Analysis of probabilistic roadmaps for path planning. *IEEE Transactions on Robotics and automation*, 14(1):166–171, 1998.
- [34] Russell Keith and Hung Manh La. Review of autonomous mobile robots for the warehouse environment. *arXiv preprint arXiv:2406.08333*, 2024.
- [35] Hyungseok Kim, Hyeongjin Kim, Seonil Lee, and Hyeonbeom Lee. Autonomous exploration in a cluttered environment for a mobile robot with 2d-map segmentation and object detection. *IEEE Robotics and Automation Letters*, 7(3): 6343–6350, 2022.
- [36] D. A. Sasi Kiran, Kritika Anand, Chaitanya Kharyal, Gulshan Kumar, Nandiraju Gireesh, Snehasis Banerjee, Ruddra dev Roychoudhury, Mohan Sridharan, Brojeshwar Bhowmick, and Madhava Krishna. Spatial relation graph and graph convolutional network for object goal navigation, 2022. URL <https://arxiv.org/abs/2208.13031>.
- [37] Jacob Krantz, Erik Wijmans, Arjun Majumdar, Dhruv Batra, and Stefan Lee. Beyond the nav-graph: Vision-and-language navigation in continuous environments. *ArXiv*, 2020.
- [38] Sharon L Laubach and Joel W Burdick. An autonomous sensor-based path-planner for planetary microrovers. In *Proceedings 1999 IEEE International Conference on Robotics and Automation (Cat. No. 99CH36288C)*, volume 1, pages 347–354. IEEE, 1999.
- [39] Binghui Li and Badong Chen. An adaptive rapidly-exploring random tree. *IEEE/CAA Journal of Automatica Sinica*, 9(2): 283–294, 2021.
- [40] Xiwen Liang, Liang Ma, Shanshan Guo, Jianhua Han, Hang Xu, Shikui Ma, and Xiaodan Liang. Cornav: Autonomous agent with self-corrected planning for zero-shot vision-and-language navigation. In *Findings of the Association for Computational Linguistics ACL 2024*, pages 12538–12559, 2024.
- [41] Yiqing Liang, Boyuan Chen, and Shuran Song. Sscnav: Confidence-aware semantic scene completion for visual semantic navigation. In *2021 IEEE international conference on robotics and automation (ICRA)*, pages 13194–13200. IEEE, 2021.
- [42] Lixing Liu, Xu Wang, Xin Yang, Hongjie Liu, Jianping Li, and Pengfei Wang. Path planning techniques for mobile robots: Review and prospect. *Expert Systems with Applications*, 227:120254, 2023.
- [43] Iker Lluvia, Elena Lazkano, and Ander Ansuategi. Active mapping and robot exploration: A survey. *Sensors*, 21(7): 2445, 2021.
- [44] Yuxing Long, Wenzhe Cai, Hongcheng Wang, Guanqi Zhan, and Hao Dong. Instructnav: Zero-shot system for generic instruction navigation in unexplored environment. *arXiv preprint arXiv:2406.04882*, 2024.
- [45] Vladimir Lumelsky and Alexander Stepanov. Dynamic path planning for a mobile automaton with limited information on the environment. *IEEE transactions on Automatic control*, 31(11):1058–1063, 1986.
- [46] Vladimir J Lumelsky and Tim Skewis. Incorporating range sensing in the robot navigation function. *IEEE transactions on Systems, Man, and Cybernetics*, 20(5):1058–1069, 1990.
- [47] Vladimir J Lumelsky and Alexander A Stepanov. Path-planning strategies for a point mobile automaton moving amidst unknown obstacles of arbitrary shape. *Algorithmica*, 2(1):403–430, 1987.
- [48] Ji Ma, Hongming Dai, Yao Mu, Pengying Wu, Hao Wang, Xiaowei Chi, Yang Fei, Shanghang Zhang, and Chang Liu. Doze: A dataset for open-vocabulary zero-shot object navigation in dynamic environments. *arXiv preprint arXiv:2402.19007*, 2024.
- [49] Steve Macenski and Ivona Jambrecic. Slam toolbox: Slam for the dynamic world. *Journal of Open Source Software*, 6(61):2783, 2021. doi: 10.21105/joss.02783. URL <https://doi.org/10.21105/joss.02783>.
- [50] Renato Martins, Dhiego Bersan, Mario FM Campos, and Erickson R Nascimento. Extending maps with semantic and contextual object information for robot navigation: a learning-based framework using visual and depth cues. *Journal of Intelligent & Robotic Systems*, 99(3):555–569, 2020.
- [51] James Clerk Maxwell. A dynamical theory of the electromagnetic field. *Philosophical Transactions of the Royal Society of London*, 155:459–512, 1865.
- [52] Farouk Meddah and Lynda Dib. E-bug: New bug path-planning algorithm for autonomous robot in unknown environment. In *Proceedings of the International Conference on Intelligent Information Processing, Security and Advanced Communication, IPAC '15*, New York, NY, USA, 2015. Association for Computing Machinery. ISBN 9781450334587. doi: 10.1145/2816839.2816864. URL <https://doi.org/10.1145/2816839.2816864>.
- [53] Ankita Mistri and Ajoy Kumar Dutta. Automated navigation of a mobile robot using ultrasonic range sensor based on modified e-bug algorithm. In *AIP Conference Proceedings*, volume 2681. AIP Publishing, 2022.
- [54] Ahmed Mohamed Mohsen, Maha Ahmed Sharkas, and Mohamed Saad Zaghlol. New real time (m-bug) algorithm for path planning and obstacle avoidance in 2d unknown environment. In *2019 29th International Conference on Computer Theory and Applications (ICCTA)*, pages 25–31. IEEE, 2019.
- [55] Anwesha Pal, Yiding Qiu, and Henrik Christensen. Learning hierarchical relationships for object-goal navigation. In *Conference on Robot Learning*, pages 517–528. PMLR, 2021.
- [56] Bao Pang, Jiahui Qi, Chengjin Zhang, Yong Song, and Runtao Yang. Analysis of random walk models in swarm robots for area exploration *. pages 2484–2489, 12 2019. doi: 10.1109/ROBIO49542.2019.8961844.
- [57] Yan Peng, Dong Qu, Yuxuan Zhong, Shaorong Xie, Jun Luo, and Jason Gu. The obstacle detection and obstacle avoidance algorithm based on 2-d lidar. In *2015 IEEE international conference on information and automation*, pages 1648–1653. IEEE, 2015.

- [58] Alec Radford, Jong Wook Kim, Chris Hallacy, Aditya Ramesh, Gabriel Goh, Sandhini Agarwal, Girish Sastry, Amanda Askell, Pamela Mishkin, Jack Clark, et al. Learning transferable visual models from natural language supervision. In *International conference on machine learning*, pages 8748–8763. PMLR, 2021.
- [59] Sharmin Rahman, Alberto Quattrini Li, and Ioannis Rekleitis. Svin2: A multi-sensor fusion-based underwater slam system. *The International Journal of Robotics Research*, 41(11-12):1022–1042, 2022.
- [60] Krishan Rana, Jesse Haviland, Sourav Garg, Jad Abou-Chakra, Ian D Reid, and Niko Suenderhauf. Sayplan: Grounding large language models using 3d scene graphs for scalable task planning. *CoRR*, 2023.
- [61] Jose Ricardo Sanchez-Ibanez, Carlos J Pérez-del Pulgar, and Alfonso García-Cerezo. Path planning for autonomous mobile robots: A review. *Sensors*, 21(23):7898, 2021.
- [62] A Sankaranarayanan and M Vidyasagar. A new path planning algorithm for moving a point object amidst unknown obstacles in a plane. In *Proceedings., IEEE International Conference on Robotics and Automation*, pages 1930–1936. IEEE, 1990.
- [63] Dhruv Shah, Błażej Osiński, Sergey Levine, et al. Lmnav: Robotic navigation with large pre-trained models of language, vision, and action. In *Conference on robot learning*, pages 492–504. PMLR, 2023.
- [64] Kensen Shi, Jory Denny, and Nancy M Amato. Spark prm: Using rrt within prms to efficiently explore narrow passages. In *2014 IEEE international conference on robotics and automation (ICRA)*, pages 4659–4666. IEEE, 2014.
- [65] Cyrill Stachniss. *Robotic mapping and exploration*, volume 55. Springer, 2009.
- [66] Jian Sun, Jie Zhao, Xiaoyang Hu, Hongwei Gao, and Jiahui Yu. Autonomous navigation system of indoor mobile robots using 2d lidar. *Mathematics*, 11(6):1455, 2023.
- [67] Allen Taflove and Susan C. Hagness. *Computational electrodynamics: the finite-difference time-domain method*, volume 67–106. Artech House, 2nd edition, 06 2000. ISBN 1-58053-076-1.
- [68] Kamilah Taylor and Steven M LaValle. I-bug: An intensity-based bug algorithm. In *2009 IEEE International Conference on Robotics and Automation*, pages 3981–3986. IEEE, 2009.
- [69] Chaoqun Wang, Lili Meng, Sizhen She, Ian M Mitchell, Teng Li, Frederick Tung, Weiwei Wan, Max Q-H Meng, and Clarence W de Silva. Autonomous mobile robot navigation in uneven and unstructured indoor environments. In *2017 IEEE/RSJ International Conference on Intelligent Robots and Systems (IROS)*, pages 109–116. IEEE, 2017.
- [70] Chaoqun Wang, Wenzheng Chi, Yuxiang Sun, and Max Q-H Meng. Autonomous robotic exploration by incremental road map construction. *IEEE Transactions on Automation Science and Engineering*, 16(4):1720–1731, 2019.
- [71] Xiuling Wang, Yong Yin, and Qianfeng Jing. Maritime search path planning method of an unmanned surface vehicle based on an improved bug algorithm. *Journal of Marine Science and Engineering*, 11(12):2320, 2023.
- [72] Kamil Wyrkabkiewicz, Tomasz Tarczewski, and Lukasz Niewiara. Local path planning for autonomous mobile robot based on apf-bug algorithm with ground quality indicator. In *Advanced, Contemporary Control: Proceedings of KKA 2020—The 20th Polish Control Conference, Łódź, Poland, 2020*, pages 979–990. Springer, 2020.
- [73] Qi-Lei Xu, Tao Yu, and Jie Bai. The mobile robot path planning with motion constraints based on bug algorithm. In *2017 Chinese Automation Congress (CAC)*, pages 2348–2352. IEEE, 2017.
- [74] Tong Xu. Recent advances in rapidly-exploring random tree: A review. *Heliyon*, 2024.
- [75] Wei Yang, Xiaolong Wang, Ali Farhadi, Abhinav Gupta, and Roozbeh Mottaghi. Visual semantic navigation using scene priors. *arXiv preprint arXiv:1810.06543*, 2018.
- [76] Naoki Yokoyama, Sehoon Ha, Dhruv Batra, Jiuguang Wang, and Bernadette Bucher. Vlfm: Vision-language frontier maps for zero-shot semantic navigation, 2023. URL <https://arxiv.org/abs/2312.03275>.
- [77] Qianfan Zhao, Lu Zhang, Bin He, Hong Qiao, and Zhiyong Liu. Zero-shot object goal visual navigation. In *2023 IEEE International Conference on Robotics and Automation (ICRA)*, pages 2025–2031. IEEE, 2023.
- [78] Chen Zhou, Jiaolong Yang, Chunshui Zhao, and Gang Hua. Fast, accurate thin-structure obstacle detection for autonomous mobile robots. In *Proceedings of the IEEE Conference on Computer Vision and Pattern Recognition Workshops*, pages 1–10, 2017.
- [79] Kaiwen Zhou, Kaizhi Zheng, Connor Pryor, Yilin Shen, Hongxia Jin, Lise Getoor, and Xin Eric Wang. Esc: Exploration with soft commonsense constraints for zero-shot object navigation. In *International Conference on Machine Learning*, pages 42829–42842. PMLR, 2023.
- [80] Jiawen Zhu and Guansong Pang. Toward generalist anomaly detection via in-context residual learning with few-shot sample prompts. In *Proceedings of the IEEE/CVF conference on computer vision and pattern recognition*, 2024.

Appendix

Some additional results are shown in the following page. Please refer to Fig. 11 for the relevant discussions. A video demonstration is provided here: <https://youtu.be/84XLM-GbhS8>.

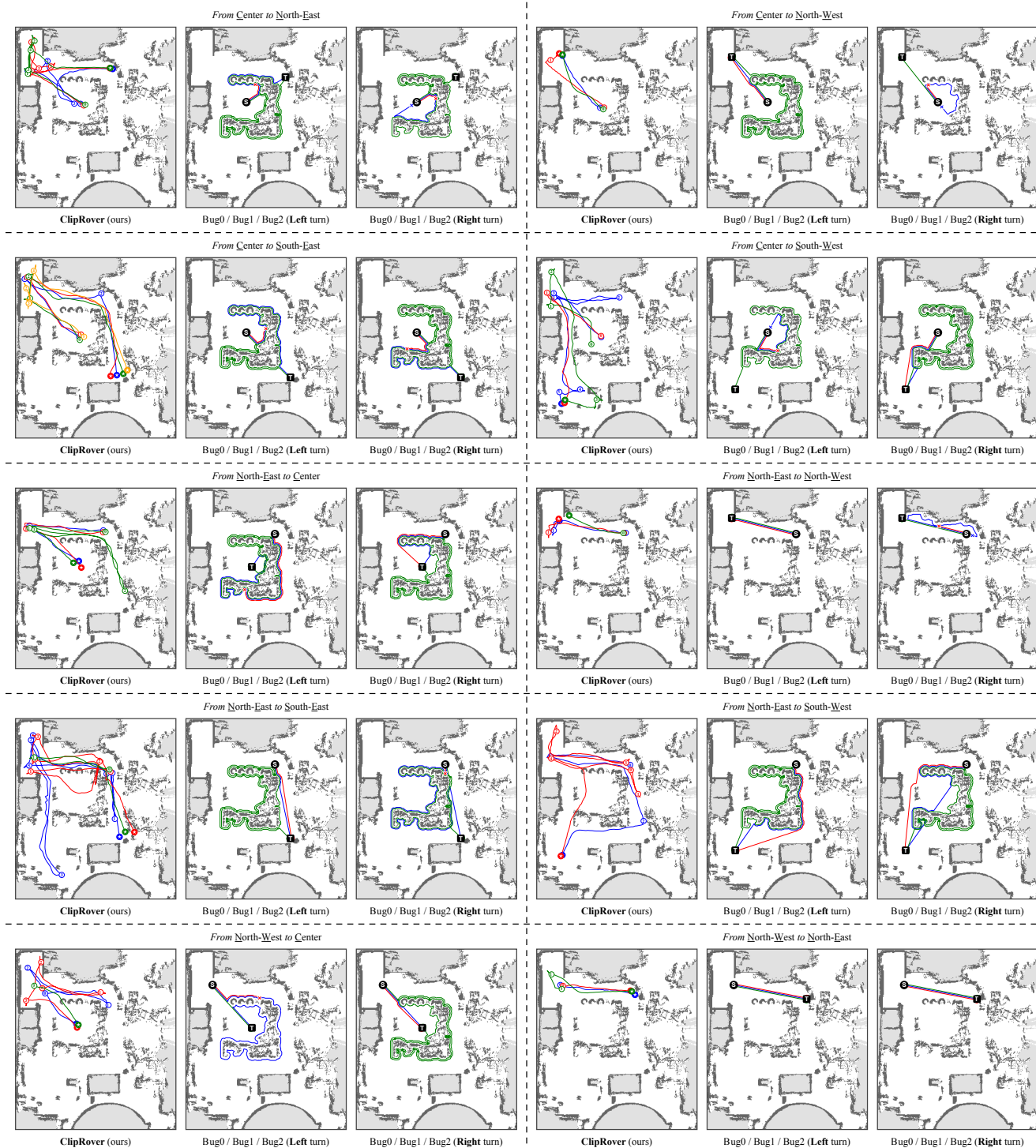


Figure 12. Qualitative comparison of all 20 trajectories for different source-target combinations among five points (C, N.W., N.E., S.W., S.E.) is illustrated (continued on the next page).

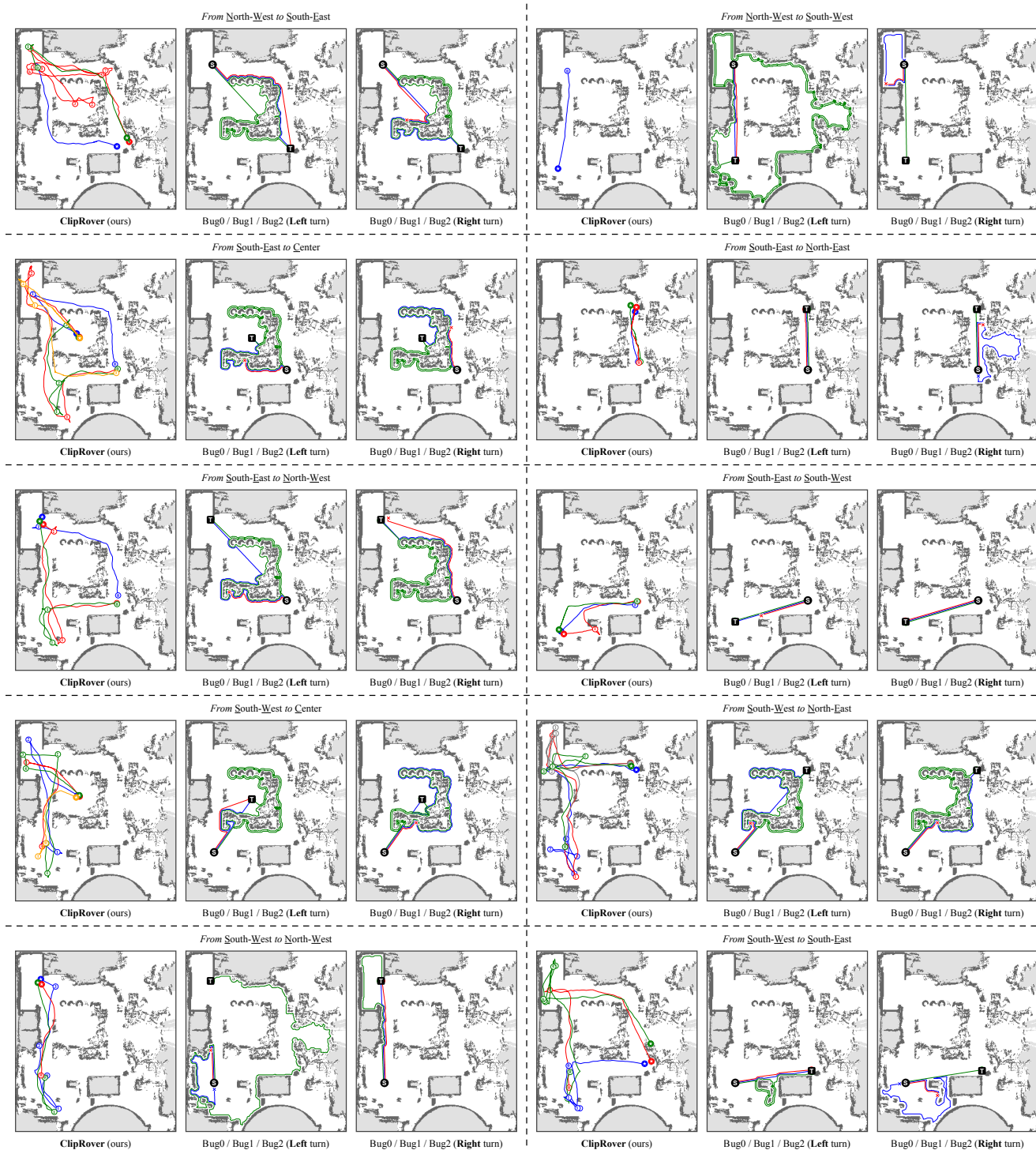


Figure 13. Qualitative comparison of all 20 trajectories for different source-target combinations among five points (C, N.W., N.E., S.W., S.E.) is illustrated. See Table 3 for a quantitative comparison.